Jeyamohan *et al.*
Advances in Bridge Engineering (2026) 7:26
https://doi.org/10.1186/s43251-026-00216-5

Advances in
Bridge Engineering

ORIGINAL INNOVATION Open Access

A differential strain-based approach for identifying prestress and moving forces in prestressed concrete bridges

Kunaratnam Jeyamohan[1*], Tommy H. T. Chan[1], Khac-Duy Nguyen[1], David P. Thambiratnam[1], Xinqun Zhu[2], Di Wu[3] and Erhua Zhang[3]

*Correspondence:
jeyamohan.kunaratnam@hdr.qut.edu.au

[1] School of Civil and Environmental Engineering, Queensland University of Technology (QUT), Brisbane 4000, Australia
[2] School of Civil and Environmental Engineering, University of Technology Sydney (UTS), Ultimo, NSW 2007, Australia
[3] Sichuan Highway Planning, Survey, Design and Research Institute Ltd, Chengdu 610031, China

Abstract

Restressing force in prestressed concrete bridges (PCBs) is reduced due to ageing, and operational and environmental loading, and it can significantly impact on their load-carrying capacity. Existing dynamic methods are insensitive to the prestress force, and the identification accuracy is significantly affected by operational environments. This paper is to develop a novel differential strain-based time-domain inverse method for prestress force identification of PCBs under moving vehicles. Both prestress and moving forces are identified simultaneously from dual strain measurements on the bridge. A Vandermonde matrix-based convolution formula is constructed to ensure the accuracy of the least squares solution for ill-posed inverse problems. The proposed method is validated using numerical studies on a two-span continuously supported prestressed concrete T-beam and verified experimentally on a simply supported box girder bridge model. Field monitoring data, together with a calibrated finite element model of a three-span continuously supported PCB, is used to further verify the performance of the proposed method. To ensure accurate formulation of the prestressed bridge–vehicle system matrix for effective force identification, modal updating with Rayleigh damping is employed in the calibration process. The results demonstrate that the proposed method can simultaneously and accurately identify both prestress and moving forces, enabling reliable real-time structural condition assessment of the bridge.

Keywords: Prestressed concrete bridge, Structural health monitoring, Prestress force, Moving force, Differential strain

1 Introduction

Prestressed concrete bridges (PCBs) are deteriorated due to ageing, and operational and environmental loads (Zhou et al. 2024; Chávez et al. 2024). The prestress losses, whether occurring individually or in combination, are attributed to factors such as shrinkage, creep (Yang 2005), steel relaxation (Yang et al. 2020), friction (Yan et al. 2021), corrosion effects (Rashetnia et al. 2018), thermal effects (Zhu et al. 2023), and freeze–thaw cycles (Cao et al. 2016) in PCBs. Therefore, the existing prestress force can have a substantial influence on the load-carrying capacity and remaining service life of PCBs (Kralovanec

© The Author(s) 2026. **Open Access** This article is licensed under a Creative Commons Attribution 4.0 International License, which permits use, sharing, adaptation, distribution and reproduction in any medium or format, as long as you give appropriate credit to the original author(s) and the source, provide a link to the Creative Commons licence, and indicate if changes were made. The images or other third party material in this article are included in the article's Creative Commons licence, unless indicated otherwise in a credit line to the material. If material is not included in the article's Creative Commons licence and your intended use is not permitted by statutory regulation or exceeds the permitted use, you will need to obtain permission directly from the copyright holder. To view a copy of this licence, visit http://creativecommons.org/licenses/by/4.0/.

Springer

et al. 2022). Identifying the actual prestress level under operational conditions is crucial for ensuring their safety and structural integrity.

A variety of methods for identifying prestress force have been proposed. These include the creep-transformed section method (Páez 2023), embedded sensor-based approach (Kim et al. 2012; Biswal and Ramaswamy 2016), vibration-based approaches (Ho et al. 2012; Breccolotti 2020), machine learning techniques (Khandel et al. 2021; Zhang et al. 2023), virtual distortion method (Xiang et al. 2016), ultrasonic technology (Hussin et al. 2020), hybrid domain adaptation approach (Talaei et al. 2025), and inverse force identification method based on structural responses (Law and Lu 2005; Lu and Law 2006; Xiang et al. 2017; Jia et al. 2023). As above, there are several practical challenges associated with accurately identifying prestress forces in PCBs. In the first place, there is inconsistent behaviour in modal parameters, particularly regarding natural frequency, which complicates measurements (Saiidi et al. 1994). Moreover, existing approaches, such as embedded sensor–based techniques cannot be widely applied to all bridges, as many PCBs lack embedded sensors and retrofitting them is often impractical due to construction constraints and long-term durability issues. In addition, the ill-conditioned nature of time-domain inverse problems poses significant challenges, necessitating the use of regularization techniques to stabilize the solution and preserve the correct subspace.

In addition to the above-mentioned approaches, some researchers have focused on assessing the residual prestress force through in-situ testing methods. These include destructive methods such as strand-cutting, crack initiation, and decompression methods, as well as non-destructive methods such as exposed strand measurement, drilled-hole techniques, and saw-cut methods (Bagge et al. 2017; Chávez et al. 2024). Furthermore, other researchers have employed static non-destructive evaluation based on vertical deflections induced by bending tests and have confirmed that the measured vertical deflections can accurately and instantaneously reflect the effects of prestress loss (Bonopera et al. 2020). Since the structural performance of PCBs is influenced by both the prestress force and the moving forces, these two parameters collectively play a critical role in governing the bridge's performance.

To ensure the accuracy of identifying moving forces on PCBs, it is also required to consider the prestress force. Overlooking the prestress force can result in significant errors in the moving force identification (Chan and Yung 2000). Several methods can be utilized for the identification of moving forces, such as time-domain method (Law et al. 1997; Chan et al. 2000), frequency time-domain method (Law et al. 1999), interpretive method-I (IM-I) (Chan et al. 2001a), bridge-weigh-in-motion (B-WIM) technique (Lai et al. 2022), statistical system model based approach (Wu and Law 2010), and interpretive method-II (IM-II) (Chan et al. 2001b). As a result of its accuracy and less computational demand, this study chose the time-domain method over all the other methods. Further efforts to identify moving forces through dynamic responses such as acceleration, rotation, and displacement are often challenged by inverse problems' ill-conditioned nature (Chen et al. 2021). To address this issue, many researchers are integrating various regularization techniques into the problem of inverse force identification. Among these techniques are the modified truncated singular value decomposition method (Chen et al. 2022), the truncated generalized singular value decomposition method (Chen et al. 2020), the modified preconditioned conjugate

gradient method (Chen et al. 2018), and the load shape function method (Wang et al. 2012). The purpose of these methods is to improve the accuracy and feasibility of identifying moving forces from bridge responses. The presence of noise is significantly high when it comes to real-time monitoring data. If these data are used to estimate the dynamic responses using finite differentiation, substantial errors are introduced in the identification of moving forces and, consequently, in the identification of prestress forces. Due to this, it is important to focus on an integrated approach that incorporates regularization and denoising techniques to enhance the accuracy of prestress force identification. Several denoising techniques have been developed to mitigate the ill-posedness inherent in signal processing. Among the techniques used to smooth data are the Butterworth filter, Savitzky-Golay filter (S-G), and Kalman filter (Luo et al. 2005; Van Breugel et al. 2020). Several advantages are associated with the S-G denoising technique, including its ability to remove noise effectively and maintain the shape of the signal, as well as its computational simplicity and speed (Acharya et al. 2016). Therefore, this study employs the convolution coefficient matrix, based on the S-G denoising technique, to enhance the identification of prestress and moving forces while minimizing computational effort.

In practice, the bridges are under traffic excitations. It is essential to identify the prestress force of PCBs under moving vehicles. Wang et al. (2024) recently proposed a methodology for identifying prestress and moving forces using Kirchhoff's plate theory in conjunction with a load shape function. In this method, the prestress force identification incorporates a mode shape Matrix that is highly sensitive to Changes in bridge stiffness. However, this sensitivity to Material degradation and strengthening effects can lead to highly ill-conditioned results when applied to real-world PCBs. Xiang et al. (2017, 2016) proposed a virtual distortion-based approach combined with a load shape function method for identifying prestress and moving forces using displacement monitoring. This method was validated using a simply supported box-girder bridge model, with periodic excitation forces applied at the bridge's mid-span. In this method, based on the sensor locations, data frequency, and sampling rate, it is necessary to develop a prestressed bridge–vehicle system matrix that incorporates the relevant degrees of freedom. This process requires significant computational effort, as the system matrix must be redeveloped each time force identification is performed. To address the high computational demands involved in reconstructing the prestressed bridge-vehicle system matrix, which are necessary due to changes in the effective stiffness of prestressed concrete bridges, Jeyamohan et al. (2024) introduced a novel method. This approach incorporates changes in effective stiffness, eliminating the need for matrix reconstruction, and utilizes a Lagrangian polynomial-based Hermitian interpolation function with only three displacement sensors. Additionally, Jeyamohan et al. (2025) proposed a substructural modelling technique-based approach for prestress and moving force identification, incorporating compressed generalized singular value decomposition. However, although both methods show promising identification accuracy using displacement monitoring, they also impose practical burdens on bridge managers due to the reliance on traditional displacement sensors, the complexity of sensor installation, and the need for reference data points (Ma et al. 2023). Together, these factors limit the widespread implementation of these methods.

In summary, current methods for identifying prestress and moving forces in PCBs face major challenges when applied under real-world conditions. Many approaches are based on simplified beam theory, which often leads to ill-conditioned results and high sensitivity to uncertainties when extended to actual bridge structures. Moreover, these methods typically require many sensors and extensive computational effort, demanding significant technical expertise for evaluating structural integrity and guiding maintenance decisions. The vast amount of data generated from multiple sensors also complicates data management for bridge authorities, increasing costs, prolonging assessment times, and potentially delaying essential maintenance, thereby posing safety risks. Existing destructive and non-destructive in-situ techniques for prestress and moving-force identification also face difficulties in large-scale bridge assessments and are impractical for continuous structural performance monitoring due to their high cost and the traffic disruptions they cause. The B-WIM technique, while capable of estimating the overall static vehicle load, cannot fully capture the dynamic effects on the bridge. Furthermore, most existing methods focus on either prestress or moving force identification individually, even though both parameters are equally crucial for accurately assessing bridge performance. Collectively, these limitations hinder the widespread implementation of current methodologies and highlight the necessity for more robust, efficient, and field-adaptable solutions. Therefore, there is a clear need to develop an enhanced, integrated approach for continuous monitoring of prestress and moving forces that addresses the challenges, enabling effective force identification while minimizing the required sensor array.

To address the challenges discussed above and provide an effective method for continuous monitoring of prestress and moving forces to assess bridge structural performance, this study introduces an enhanced time-domain integrated approach for identifying these forces using only dual strain responses (strain data from two locations) at selected elements along the longitudinal direction of PCBs. In this approach, a convolution matrix constructed using a Vandermonde matrix is incorporated into the inverse identification process to maintain the correct subspace (the identified time-history forces correspond to the physically valid structural responses of the bridge, with the ill-posedness effectively minimized) and ensure accurate estimation. The appropriate convolution matrix is selected by introducing a local pseudo-force ratio and comparing it with the shape function derived from a Lagrangian polynomial-based Hermitian interpolation function. Unlike existing methods that require separate procedures, different sensor types, and large amounts of data for prestress and moving force identification, the proposed integrated approach allows simultaneous estimation of both parameters, thereby reducing data volume, computation time, and complexity. Furthermore, while traditional approaches often model PCBs as beam-type structures, leading to ill-conditioning and sensitivity to uncertainties, the method proposed in this study is readily adaptable to real bridge conditions, where structural behaviour more closely resembles that of a plate-like system. Moreover, the proposed approach enables reliable time-domain monitoring of the actual prestress force with minimal effort. In contrast, standard prestress-loss formulas require extensive information from multiple construction stages and in-situ tests, which makes them impractical for real-time, continuous monitoring of the actual prestress forces. This study also addresses practical challenges in field instrumentation. The method

eliminates the need for multiple displacement sensors, avoids difficulties associated with placing sensors on the soffit of PCBs, and reduces the likelihood of requiring road closures. Moreover, guidance on optimal sensor placement is provided, recommending positions near mid-span rather than near supports to enhance identification accuracy. Ultimately, this streamlined and efficient sensing-based approach, relying solely on dual strain data, significantly reduces computational demands and sensor requirements, greatly simplifying implementation and management for bridge administrators.

2 Inverse identification of prestress and moving forces using dual strain responses and a convolution matrix

2.1 Dynamic equilibrium equation for moving force under prestressing conditions

Figure 1 illustrates the configuration of a PCB with prestressing conditions under the moving force.

The dynamic equilibrium of the prestressed beam under a moving force, formulated using the Euler–Bernoulli beam model, is given in Eq. (1) (Lu & Law 2006).

$$\mathbf{M}\ddot{\boldsymbol{x}} + \mathbf{C}\dot{\boldsymbol{x}} + \overline{\mathbf{K}}\boldsymbol{x} = \mathbf{Z} \cdot \mathbf{F}(t) \tag{1}$$

where $\boldsymbol{x}$, $\dot{\boldsymbol{x}}$, and $\ddot{\boldsymbol{x}}$ represent the displacement, velocity, and acceleration vectors, respectively. $\mathbf{M}$, $\mathbf{C}$, and $\overline{\mathbf{K}}$ are respectively the mass, damping, and stiffness matrices of the prestressed concrete beam where the stiffness matrix incorporates the compression softening effect (when a beam is subjected to axial compression, its natural frequency decreases due to the compression softening effect. As a result, the equivalent flexural stiffness of a prestressed member becomes lower than that of an identical beam without axial compression. Hence, the contribution of the axial load leads to a reduction in the effective stiffness matrix rather than an increase) (Tse FS et al. 1978; Chan and Yung 2000). $\mathbf{Z}$ is the mapping matrix for the moving force, and the vector $\mathbf{F}(t)$ represents the moving force, characterized by a discrete time history. Equation 1 can be rewritten by representing the softening effect as the equivalent external pseudo forces ($\boldsymbol{\Upsilon}$) as follows (Xiang et al. 2017),

$$\mathbf{M}\ddot{\boldsymbol{x}} + \mathbf{C}\dot{\boldsymbol{x}} + \mathbf{K}\boldsymbol{x} = \mathbf{Z} \cdot \mathbf{F}(t) + \boldsymbol{\Upsilon} \tag{2}$$

where $\mathbf{K}$ represents the stiffness matrix of the PCB prior to the introduction of prestressing (at zero prestress force). The equivalent external pseudo force matrix is expressed as (Chan and Yung 2000),

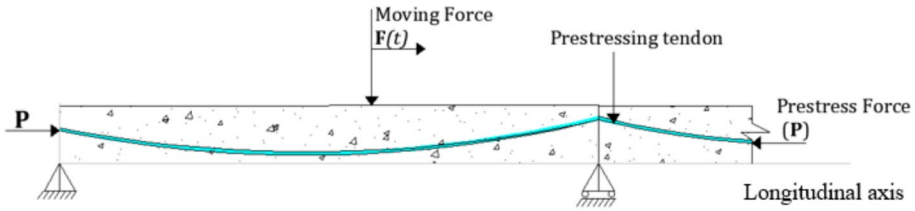


Fig. 1 PCB with a prestressing arrangement subjected to a moving force

$$\Upsilon = \frac{\mathbf{P}}{30l}\begin{bmatrix} 30 & 0 & 0 & -30 & 0 & 0 \\ 0 & 36 & 3l & 0 & -36 & 3l \\ 0 & 3l & 4l^2 & 0 & -3l & -l^2 \\ -30 & 0 & 0 & 30 & 0 & 0 \\ 0 & -36 & -3l & 0 & 36 & -3l \\ 0 & 3l & -l^2 & 0 & -3l & 4l^2 \end{bmatrix} \boldsymbol{x} \tag{3}$$

where **P** represents the prestress force, and l denotes the length of the considered element. The unknown external pseudo-forces from prestress, along with nodal forces induced by moving forces, can be identified by applying the Duhamel integral within the convolution process, which accounts for all external forces and their associated impulse response functions as,

$$x_k(t) = \int_0^t h^k(t-\tau) f(\tau) d\tau k = 1, 2, 3..... \tag{4}$$

where $x_k(t)$ is the sensor responses at the k^{th} sensor, $h^k(t-\tau)$ is the impulse response between the force location and the sensor, and $f(\tau)$ is the unknown external force. The convolution is approximated by multiplying the external force and impulse response matrices as,

$$\mathbf{Y} = \mathbf{B} \cdot \mathbf{F}^e \tag{5}$$

where **B** represents the impulse response matrix (sensitivity to the flexural stiffness of the bridge) for the equivalent external nodal forces ($\mathbf{F}^e$) due to unknown prestress and moving forces, and **Y** denotes the measured structural responses. In the proposed inverse force identification approach, the bridge is assumed to exhibit uniform linear elastic behaviour with isotropic material properties. Damping is modelled using Rayleigh damping, and geometric nonlinearity is considered during the construction of the impulse response matrix based on the finite element (FE) model.

2.2 Identification of prestress force using dual strain responses incorporating a pseudo-prestress response matrix and a convolution matrix

This study proposes a method for identifying prestress forces using dual strain responses by attaching strain sensors at two locations along the longitudinal direction of the PCB. To accurately identify the prestress force from the measured strain data, a virtual strain response matrix is constructed. The concept of strain difference at a specific element is introduced to minimize errors in constructing the virtual strain response matrix using a FE model. This approach helps mitigate computational errors in obtaining strain responses caused by external pseudo-forces, as well as uncertainties encountered during real-bridge monitoring. The entire bridge can be discretised into multiple elements, and the effect of the prestress force can be transformed into equivalent external pseudo-forces at each node of the elements. The arrangement of external pseudo forces and element marking is depicted in Fig. 2.

By introducing external pseudo-forces along the PCB, the relationship between the measured strain response and applied external pseudo-force at the i^{th} location is established through the introduction of a virtual strain response matrix at the i^{th} location, as shown in Eq. (6) based on Eq. (5).

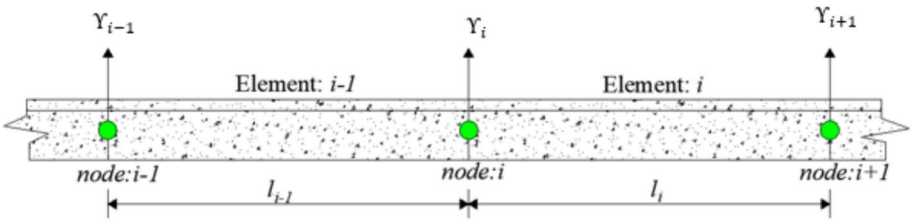


Fig. 2 The arrangement of external pseudo forces, along with node and element markings

$$\varepsilon_{e,i} = S_i \cdot \Upsilon_i \tag{6}$$

where $\varepsilon_{e,i}$ is the bending strain obtained from the FE model at the i^{th} node under the respective external pseudo force Υ_i, and S_i is the corresponding virtual strain response matrix at the i^{th} node, resampled to match the sensor's sampling frequency. The virtual strain response matrix is generated by applying random external excitation at various locations along the longitudinal direction of the PCB and obtaining the corresponding bending strain responses using a calibrated FE model. The strain difference at element $i-1$ ($\delta\varepsilon_{e,i-1}$) can then be expressed as shown in Eq. (7).

$$\delta\varepsilon_{e,i-1} = \varepsilon_{e,i} - \varepsilon_{e,i-1} = (S_i - S_{i-1})\Upsilon_i \tag{7}$$

where $\varepsilon_{e,i-1}$ represents the bending strain at $i-1^{th}$ location under the respective external pseudo-force (Υ_i), and S_{i-1} is the strain response matrix at $i-1^{th}$ node. By utilizing the geometrical stiffness matrix induced by the prestress force, the relationship between the external pseudo-force and the prestress force can be established using the translational and rotational displacements obtained from the FE model, as demonstrated in Eq. (8), which can be constructed using Eq. (3).

$$\frac{\Upsilon_i}{P_i} = \begin{bmatrix} \frac{-36}{30l_{i-1}} & \frac{-1}{10} & (\frac{36}{30l_{i-1}} + \frac{36}{30l_i}) & 0 & \frac{-36}{30l_i} & \frac{1}{10} \end{bmatrix} \begin{Bmatrix} x_{t,i-1} \\ x_{r,i-1} \\ x_{t,i} \\ x_{r,i} \\ x_{t,i+1} \\ x_{r,i+1} \end{Bmatrix} \tag{8}$$

Where $x_{t,i}$ and $x_{r,i}$ represent the translational and rotational displacement responses at node i, l_i is the element length, and P_i is the equivalent prestress force corresponding to the equivalent external pseudo force (Υ_i). Using Eq. (8), the pseudo-prestress force ratio response matrix (Ω_i) at node i can be estimated, as presented in Eq. (9).

$$\frac{\Upsilon_i}{P_i} = \Omega_i \tag{9}$$

To account for the local pseudo-force effect induced by the prestress force along the bridge model, a mapping matrix for prestress force identification (Z^p_{i-1}) is constructed and introduced in Eq. (7), incorporating the pseudo-prestress force ratio response matrix derived from Eq. (9). The modified relationship for the differential strain (difference in strain between two sensor locations) at a specific element, considering the entire bridge model, is presented in Eq. (10).

$$\delta\varepsilon_{e,i-1} = Z^{p}_{i-1} \cdot \Omega_i (S_i - S_{i-1}) P_i \tag{10}$$

where $\delta\varepsilon_{e,i-1}$ represents the differential strain at element $i-1$. Consequently, identifying the prestress force using the differential strain at a specific element becomes an inverse problem, as illustrated in Eq. (11), which is derived from Eq. (10).

$$\delta\varepsilon_{e,i-1} = D_{i-1} \cdot P_i \tag{11}$$

where D_{i-1} represents the differential virtual strain response matrix at element $i-1$, which is given by $Z^{p}_{i-1} \cdot \Omega_i (S_i - S_{i-1})$. Thus, the unknown prestress force at a specific element, utilizing the dual strain responses of that element, can be expressed as shown in Eq. (12).

$$P_i = {D_{i-1}}^{-1} \cdot \delta\varepsilon_{e,i-1}; \text{ where } \delta\varepsilon_{e,i-1} = \varepsilon_{e,i} - \varepsilon_{e,i-1} \tag{12}$$

The differential virtual strain response matrix can be constructed using a calibrated FE model by applying known random external pseudo-forces and measuring the bending strain responses at each node. In this way, the differential strain at the selected element, along with the mapping matrix, can be developed by applying known random external pseudo-forces at each node of the bridge model. The general form for prestress force ($\mathbf{P}$) identification at any element, using the differential strain response matrix ($\boldsymbol{\delta\varepsilon}$), can then be expressed as shown in Eq. (13).

$$\mathbf{P} = \mathbf{D}^{-1} \cdot \boldsymbol{\delta\varepsilon} \tag{13}$$

where $\mathbf{D}$ represents the differential virtual strain response matrix for the entire bridge, encompassing all elements. To improve the accuracy of prestress force identification using differential strain responses in the inverse problem, the differential virtual strain response matrix can be refined by obtaining a least-squares solution. This is achieved by incorporating the convolution matrix into the identification of prestress force, as shown in Eq. (14).

$$\mathrm{P}\varepsilon R^{nMIN}\{||\mathbf{D} \cdot \mathbf{P} - \boldsymbol{\delta\varepsilon}||_2^2 + ||\mathbf{C}_w \cdot \mathbf{P}||_2^2 \tag{14}$$

where $\mathbf{C}_w$ denotes the convolution matrix. Further refinement of the differential virtual strain response matrix is achieved by assuming the prestress force remains consistent throughout the bridge structure. The matrix is refined by calculating the prestress force for each element using differential virtual strain responses from the FE model under random external pseudo-forces. By selecting the appropriate convolution matrix, a least-squares solution for prestress force identification can be obtained. This approach allows for a more accurate derivation of the refined differential virtual strain response matrix ($\mathbf{D}^{*}$), enhancing the accuracy of prestress force identification as shown in Eq. (15).

$$\mathbf{P}_{refined} = \mathbf{D}^{*-1} \cdot \boldsymbol{\delta\varepsilon} \tag{15}$$

where $\mathbf{P}_{refined}$ represents the refined prestress force across the entire bridge.

2.3 Inverse identification of moving forces using dual strain responses and a convolution matrix

Using the dynamic equilibrium from Eq. (1) and performing the convolution as shown in Eqs. (4) and (5), this study presents a methodology for identifying moving forces ($\mathbf{F}(t)$) as an inverse problem, utilizing differential strain responses ($\boldsymbol{\delta\varepsilon}$), as illustrated in Eq. (16).

$$\mathbf{F}(t) = \mathbf{H}^{-1} \cdot \boldsymbol{\delta\varepsilon} \tag{16}$$

where $\mathbf{H}$ represents the prestressed bridge-vehicle system matrix used for moving force identification. The matrix $\mathbf{H}$ is constructed based on a novel approach, utilizing both the refined mapping matrix ($\mathbf{Z}^*$) and the refined differential virtual strain response matrix ($\boldsymbol{\delta}\mathbf{s}^*$), as outlined in Eq. (17).

$$\mathbf{H} = \mathbf{Z}^* \cdot \boldsymbol{\delta}\mathbf{s}^* \tag{17}$$

To develop the refined prestressed bridge-vehicle system matrix for moving force identification, a calibrated FE model is used by introducing known random external pseudo-forces ($\boldsymbol{\Upsilon}$) and obtaining differential strain responses at specific locations ($\boldsymbol{\delta\varepsilon}_e$). By repeating this process for all nodes, a differential virtual strain response matrix for the entire bridge, incorporating all nodes, can be constructed, as shown in Eq. (18).

$$\boldsymbol{\delta\varepsilon}_e = \mathbf{Z} \cdot \boldsymbol{\delta}\mathbf{s} \cdot \boldsymbol{\Upsilon} \tag{18}$$

where $\boldsymbol{\delta}\mathbf{s}$ represents the strain difference response matrix for moving force identification, obtained under random external pseudo forces. $\mathbf{Z}$ is the mapping matrix, aligned with the shape function matrix, to capture the dynamic behaviour of the entire bridge. The primary goal of this study is to use differential strain responses to minimize computational errors in constructing the prestressed bridge-vehicle system matrix. Additionally, the matrix is further enhanced by incorporating the convolution matrix into Eq. (16), improving both the accuracy of the inverse problem solution and preserving the correct subspace for moving force identification. As a result, the least squares solution of the linear algebraic equation is presented in Eq. (19).

$$\mathbf{p}_{u \varepsilon R^n}{}^{MIN} \{ || \mathbf{Z} \cdot \boldsymbol{\delta}\mathbf{s} \cdot \boldsymbol{\Upsilon} - \boldsymbol{\delta\varepsilon}_e | |_2^2 + || \mathbf{C}_w \cdot \boldsymbol{\Upsilon} | |_2^2 \} \tag{19}$$

By selecting an appropriate convolution matrix ($\mathbf{C}_w$), the differential strain response matrix and the corresponding mapping matrix under random external pseudo-forces can be refined based on the FE model study. This refinement enables the construction of a more accurate mapping matrix and differential virtual strain response matrix for performing moving force identification. Additionally, this novel methodology reduces the computational effort required for moving force identification by utilizing only dual strain measurements, compared to existing methods.

2.4 Construction of the convolution matrix for enhancing inverse force identification

This section introduces the use of a convolution matrix to enhance the inverse identification of prestress and moving forces and to ensure accurate subspace determination by refining the construction of the differential virtual strain response matrix. The primary function of the convolution matrix can be written in the form as shown in Eq. (20) (Acharya et al. 2016).

$$\eta_{j,smoothed} = \sum_{w=\frac{1-i}{2}}^{w=\frac{i-1}{2}} C_w \eta_{j+w};\ \frac{i+1}{2} \le j \le n - \frac{i-1}{2} \tag{20}$$

where the parameter to be smoothed is denoted as η, i represents the set of convolution coefficients, w is the window size, C_w denotes the convolution coefficients, j represents the set of data points, and n is the number of data samples. The convolution matrix can be expressed as shown in Eq. (21), based on the Vandermonde matrix ($\mathbf{J}$).

$$\mathbf{C}_w = \left(\mathbf{J}^{\mathrm{T}}\mathbf{J}\right)^{-1}\mathbf{J}^{\mathrm{T}} \tag{21}$$

To derive the convolution coefficients, the polynomial of a given degree is defined in Eq. (22).

$$\eta = g_0 + g_1 z + g_2 z^2 + \cdots + g_k z^k \tag{22}$$

where z represents the set of elements within a specific window size (e.g. $w = 7$: z=-3, -2, −1, 0, 1, 2, 3) and g_0, g_1, g_2... are the coefficients of the polynomial. The coefficients vector of the polynomial ($\mathbf{g}$) can be written by incorporating the Vandermonde matrix as shown in Eq. (23).

$$\mathbf{g} = \left(\mathbf{J}^{\mathrm{T}}\mathbf{J}\right)^{-1}\mathbf{J}^{\mathrm{T}}\boldsymbol{\eta} \tag{23}$$

The Vandermonde matrix can be constructed such that the i^{th} row contains the values $1, z_i, z_i^2, \ldots\ldots z_i^k$. Therefore, by solving the above equation, convolution coefficients can be obtained for the required window size. It is important to consider the polynomial order and window size when determining the effectiveness of noise reduction through the convolution matrix. The accuracy and correct subspace primarily depend on selecting the appropriate window size. The study adopts a quadratic (second order) polynomial because it helps balance between noise smoothing and preservation of key signal features. A second-degree polynomial was selected as the lowest-order fit that captures the both linear and curvature trends in local data with sufficient accuracy for the measured response; higher-order fits provided negligible improvement while increasing computational demand and risking overfitting/oscillatory behaviour (Savitzky and Golay 1964; Staggs 2005).

2.4.1 Selection of appropriate window size for the convolution matrix

Selecting the appropriate window size for the convolution matrix is crucial for the accurate identification of both prestress force and moving force. The optimal window size is primarily governed by the bridge response characteristics (i.e., the structural condition) that define the dominant response scale to be captured. In contrast, the signal-to-noise

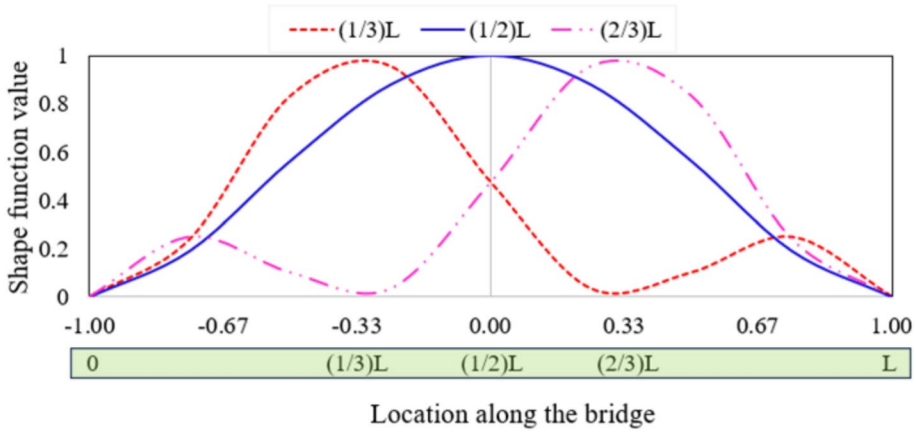


Fig. 3 The variation of the shape function under a specific external pseudo force at different locations (1/3) L, (1/2) L, and (2/3) L of the bridge

Convolution coefficients																	N	*i*
17	16	15	14	13	12	11	10	9	8	7	6	5	4	3	2	1	0	
Values ↓																		
															-3	12	17	35	5
													-21	14	39	54	59	231	9
					-253	-138	-33	62	147	222	287	343	387	422	447	462	467	5175	25
-528	-363	-208	-63	72	197	312	417	512	597	672	737	792	837	872	897	912	917	14245	35
Values ↑																		
-17	-16	-15	-14	-13	-12	-11	-10	-9	-8	-7	-6	-5	-4	-3	-2	-1	0	
Convolution coefficients																	N	*i*

Fig. 4 The convolution coefficients of the $\mathbf{C}_5$, $\mathbf{C}_9$, $\mathbf{C}_{25}$, and $\mathbf{C}_{35}$ convolution matrices

ratio and sensor configuration mainly affect the accuracy and robustness of the window-size estimation, potentially causing small variations in the identified convergence point. Therefore, this study determines one window size for each specific case study by scanning candidate window sizes and selecting the smallest value beyond which the local pseudo-force ratio stabilizes (converges). This choice yields stable results with minimal computational demand while maintaining identification accuracy. To address this, the study introduces a technique called the local pseudo-force ratio, which helps determine the suitable window size. The definition of this ratio is provided in Eq. (24).

$$\eta_{i-1} = \frac{\left[\frac{\Upsilon}{P}\right]_i}{\left[\frac{\Upsilon}{P}\right]_{i-1}} = \frac{\Omega_i}{\Omega_{i-1}} \tag{24}$$

The theoretical local pseudo-force ratio is defined using the shape function at specific locations on the bridge, developed through a Lagrangian polynomial-based Hermitian interpolation function. The theoretical shape functions, based on external pseudo forces applied at locations (1/3) L, (1/2) L, and (2/3) L of the bridge, are illustrated in Fig. 3.

By improving the local pseudo-force ratio using different window sizes, the error can be estimated by comparing it with the theoretical local pseudo-force ratio derived from the shape function. Through this comparison of the estimated error with the theoretical

ratio, the appropriate window size for the convolution matrix can be determined. The convolution coefficients of the $\mathbf{C}_5$, $\mathbf{C}_9$, $\mathbf{C}_{25}$, and $\mathbf{C}_{35}$ convolution matrices are presented in Fig. 4. In this Fig. 4, **N** represents the normalization value.

2.5 Overall methodology flowchart for prestress and moving force identification

The overall methodology of the proposed dual strain response-based approach for identifying prestress and moving forces in prestressed concrete bridges is clearly outlined in the flowchart shown in Fig. 5. The process begins with constructing the prestressed bridge-vehicle system matrix for prestress and moving force identification using strain responses measured at two locations along the beam, under random external pseudo forces. Model calibration can be performed through modal testing by matching measured and simulated natural frequencies. Specifically, the first three modal frequencies are extracted from the measured acceleration records using the fast Fourier transform, and the FE model is then updated by iteratively adjusting the key parameters, primarily the elastic modulus and mass density. By incorporating Rayleigh damping, the damping representation is also updated indirectly through these two key parameters. The updating process aims to minimise the discrepancy between each pair of measured and analytical modal frequencies. To further streamline the calibration, the measured strain response under known static vehicle weight is also incorporated. Using the overall static vehicle weight together with the corresponding strain data provides an additional constraint for estimating the elastic modulus, which reduces the search space and lowers the computational burden of the iterative updating procedure.

Next, the differential strain responses at specific elements are estimated to construct the bridge-vehicle system matrix for moving force identification. The process is further refined by incorporating a convolution matrix into the identification method. Finally, by measuring the strain responses at each node of a particular element and inputting

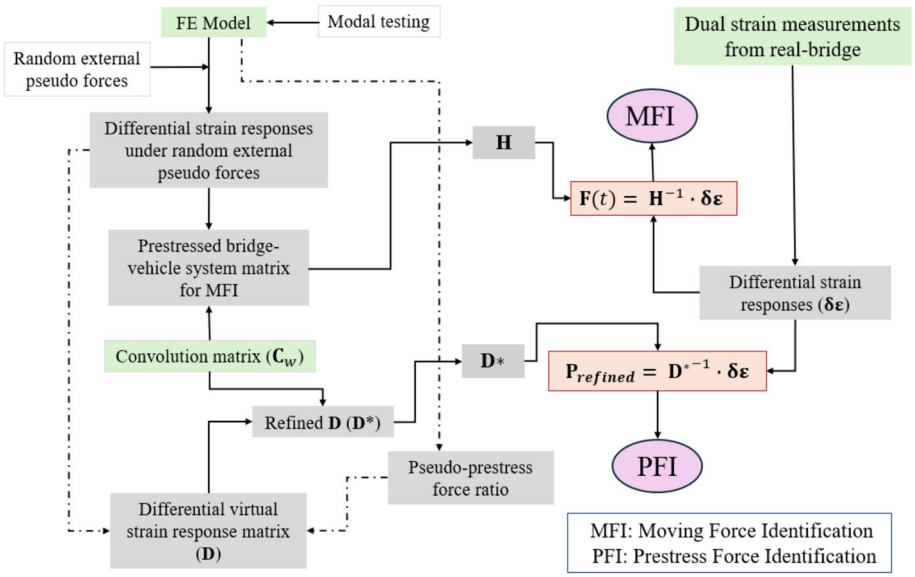


Fig. 5 The overall methodology for identifying prestress forces and moving forces using dual strain measurements

the differential strain responses, the moving forces can be identified effectively, as discussed in Sect. 2.3. Furthermore, to perform prestress force identification, a differential virtual strain response matrix is constructed using strain responses obtained under random external pseudo forces, incorporating the pseudo-prestress force ratio concept as discussed in Sect. 2.2. By integrating the convolution matrix, a refined differential virtual strain response matrix can be created. Using the differential strain response from the real bridge (by utilizing strain data from two sensor locations) monitoring for the selected element, prestress force identification can then be conducted. The construction of the convolution matrix has been detailed in Sect. 2.4.

3 Validation 1: Prestress force and moving force identification in continuously supported prestressed concrete beam (Numerical study)

3.1 Continuously supported prestressed concrete T-beam for numerical study

As shown in Fig. 6, a continuously supported prestressed concrete T-beam with two 20-m spans is selected for the numerical study. The T-beam is modelled in Abaqus using C3D8R solid elements, with an element size of 40 mm determined from the convergence study. The bridge has an elastic modulus of 34 GPa and a density of 2500 kg/m^3. The sampling frequency for this study is 200 Hz, with a measurement duration of 1 s.

Table 1 shows the arrangement and position of the parabolic tendon in the first span of a continuously supported prestressed concrete beam (the 1 st and 2nd spans are symmetric). In this study, two levels of prestress force, 2000 kN and 3000 kN, are considered, ensuring that the proposed prestress forces remain below the critical buckling load of the concrete T-beam. The strain gauge arrangement for this study is shown in Fig. 7. The sensor locations are selected to include various positions and element lengths, ensuring the proposed method's applicability across different sensor arrangements.

The prestress force is applied to the ABAQUS model using an equivalent load-balancing technique, based on the relationship for a uniformly distributed force, which is defined as $8Pe/l^2$, where e represents the sag, P is the prestress force, and l is the length of the parabolic profile.

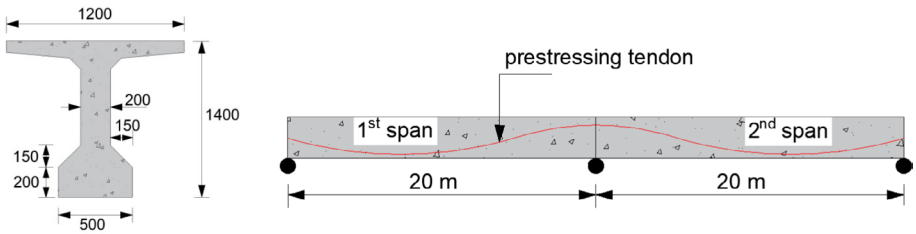


Fig. 6 Continuously supported prestressed concrete T-beam (**a**) cross-sectional view (**b**) longitudinal view

Table 1 Parabolic tendon arrangement in the continuously supported prestressed concrete T-beam

Longitude (mm)	**0**	**3330**	**6666**	**10,000**	**13,760**	**17,200**	**20,000**
Distance from the bottom of the beam (mm)	682	294	140	207	560	1000	1120

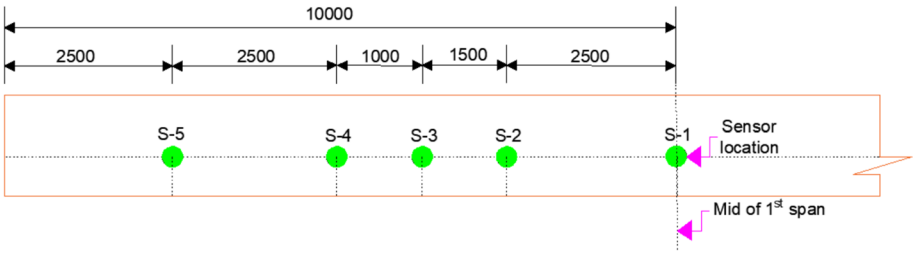


Fig. 7 The arrangement of strain gauges in the continuously supported prestressed concrete T-beam for the numerical study

Initially, a modal analysis was conducted, and the Rayleigh damping coefficients were estimated using the first two natural frequencies, which characterise the primary bridge response under service-level vibrations (Yau et al. 1999; Ma et al. 2019). It could be estimated using the following Eq. (25) by estimating the frequencies (Rahman and Gupta 2020).

$$\zeta_n = \frac{\rho}{2}\frac{1}{\omega_n} + \frac{\varphi}{2}\omega_n \tag{25}$$

where ω_n is the natural angular frequency at n^{th} mode and ζ_n is the damping ratio. Therefore, damping coefficients can be determined by considering the damping ratios of the i^{th} and j^{th} modes, as illustrated in the following Eq. (26).

$$\frac{1}{2}\begin{bmatrix} 1/\omega_i & \omega_i \\ 1/\omega_j & \omega_j \end{bmatrix}\begin{Bmatrix} \rho \\ \varphi \end{Bmatrix} = \begin{Bmatrix} \zeta_i \\ \zeta_j \end{Bmatrix} \tag{26}$$

where ω_i and ω_j are the natural angular frequencies at i^{th} and j^{th} modes. As part of this study, the first and second modes of vibration are considered, and the frequencies of the first and second modes are 4.108 Hz and 5.074 Hz, respectively. For both modes, a damping ratio of 0.02 was adopted to represent typical in-service damping of concrete bridges under traffic excitation (Law and Lu 2005; Ma et al. 2019). Therefore, coefficients p and φ are estimated as 0.09 and 0.0044, respectively, and used in the proposed FE-based approach for determining prestress force. Figure 8 presents the mesh view and deformation contour of the prestressed continuously supported T-beam.

In the numerical study, various bridge surface conditions and vehicle speeds were considered, as outlined in Table 2. The bridge surface conditions were classified as very good, average, and poor, as detailed in the table below. The moving force input for the numerical

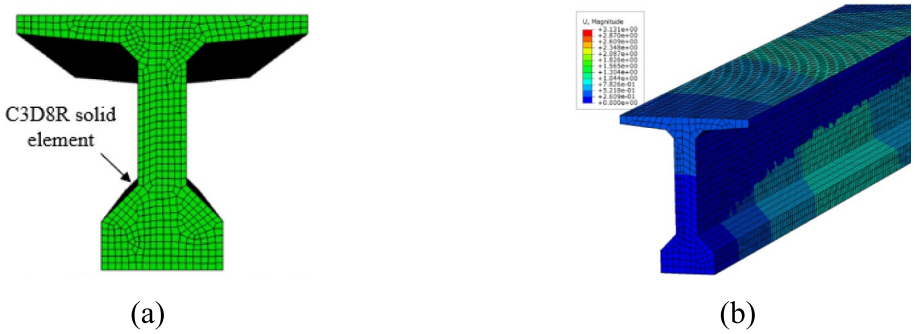


Fig. 8 FE model of a continuously supported prestressed concrete T-beam (**a**) mesh view (**b**) deformation contour

Table 2 Moving force conditions with varying bridge surface conditions and vehicle speeds in the continuously supported prestressed concrete T-beam

Cases	Bridge surface condition	Vehicle speed (m/s)
MF-C1	Very Good	20
MF-C2	Average	
MF-C3	Poor	
MF-C4	Very Good	10
MF-C5	Average	
MF-C6	Poor	

study is estimated based on the bridge surface condition and vehicle speeds, as explained in Sect. 3.2.

3.2 Estimation of moving force as input for numerical study

In this study, the moving force is generated by considering the bridge surface condition, vehicle speed, and the stiffness and damping of the vehicle's suspension system. This moving force serves as the input for the numerical analysis to obtain strain measurements. During the process of moving force identification, the study relies solely on the strain measurements obtained from the numerical analysis as the input parameter. Consequently, the actual moving force used in the numerical study is estimated using Eq. (28) (Agostinacchio et al. 2014; Van Van and Thanh Tung 2023). The equation below only accounts for the effect of relative displacement caused by road surface conditions on the vehicle, as the primary focus of this study is to develop the moving force input for numerical analysis. The relative displacement on the vehicle is taken equal to the road surface roughness profile as shown in the Fig. 9.

$$F(t) = F_{Static} + F_{Suspension} + F_{Damping} \tag{27}$$

$$F(t) = F_{Static} + K_v \cdot y(t) + C_v \cdot \dot{y}(t) \tag{28}$$

where F_{Static} is the static force of the vehicle, $F_{Suspension}$ is the force induced by the vehicle's suspension system, and $F_{Damping}$ is the force induced by the damping effect of the vehicle. K_V represents the stiffness of the vehicle's suspension system, C_V denotes the damping of the suspension system, and y represents the relative displacement of the vehicle, which is assumed to be equivalent to the road surface roughness profile ($r(x)$). The road surface roughness is estimated using the following relationship as shown in Eq. (29) (Agostinacchio et al. 2014).

$$r(x) = \sum_{i=1}^{N} \sqrt{\Delta n}.2^k.10^{-3}.\left(\frac{n_0}{i.\Delta n}\right)\cos(2\pi.i.\Delta n.x + \varnothing_i) \tag{29}$$

where, k is a constant that varies from 3 to 9 depending on the road class A to H (based on the ISO 8608 classification), N is the number of data points, Δn is equal to $\frac{1}{L}$, where L is the span of the bridge, and n_0 is equal to 0.1 cycles per meter. $\varnothing_i$ is the random phase angle, varying between 0 and 2π. By expressing the vehicle's moving distance x in terms

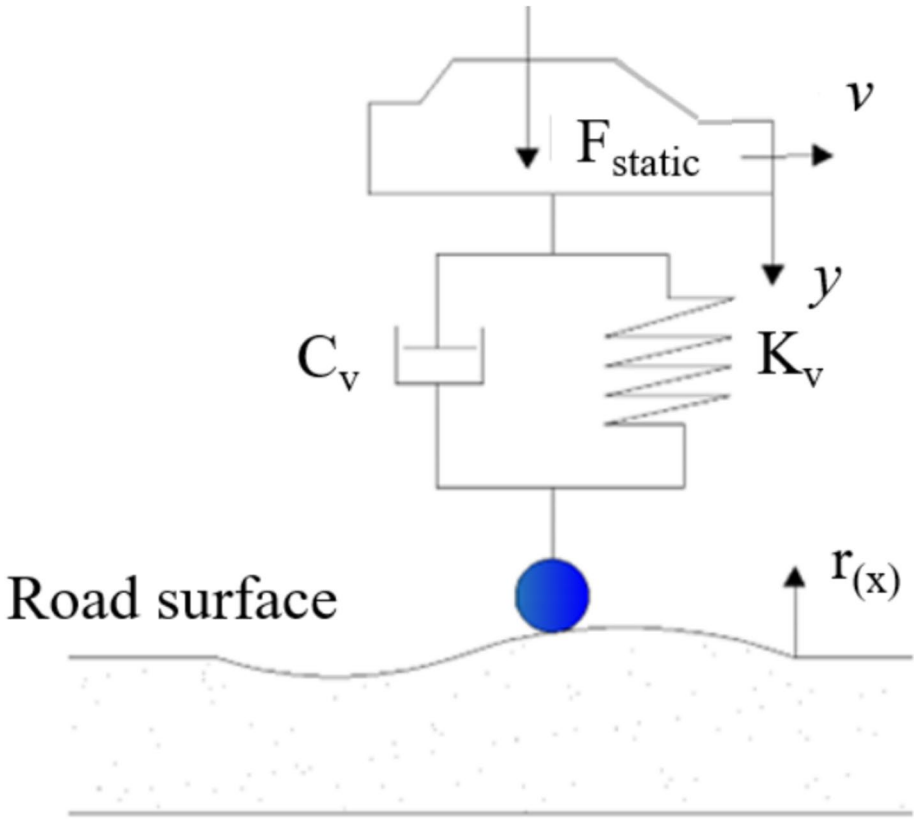


Fig. 9 Quarter car model arrangement

of speed v and time t, where $x = v \cdot t$, the road surface roughness equation is transformed into a time history equation. The k values are chosen based on different bridge surface conditions: 3 for very good, 6 for average, and 8 for poor. Using these values, a road surface profile is developed, as shown in Fig. 10, to estimate the input moving force for the numerical study. Additionally, the stiffness of the vehicle's suspension system is set at 6.7×10^6 N/m, the damping at 7.82×10^4 N/m/s, and the vehicle's static force is taken as 175 kN.

Based on this approach, road surface roughness over time and the moving force are estimated for different vehicle speeds and various road surface conditions. These

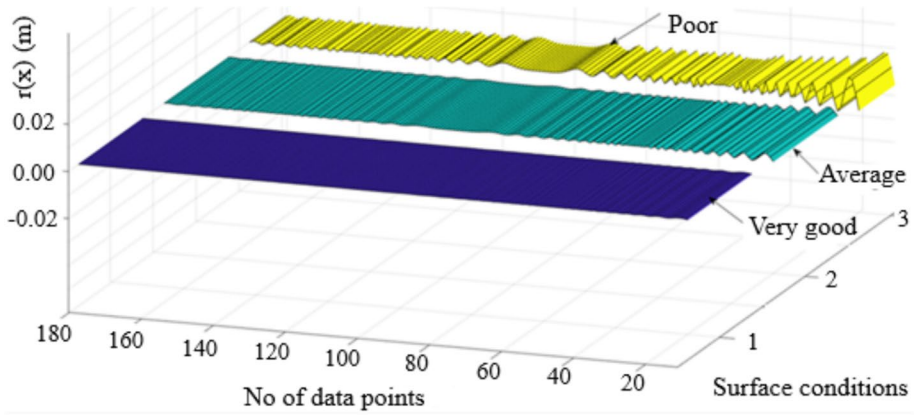


Fig. 10 Longitudinal bridge surface profile under varying bridge surface conditions

estimates are then used as inputs in the numerical analysis to obtain strain measurements. The road surface roughness and moving force estimated at a vehicle speed of 20 m/s are presented in Fig. 11.

3.3 Prestress force and moving force identification using dual strain measurements in continuously supported prestressed concrete T-beam

Strain measurements were obtained at all sensor locations for each case and both stages of prestressing. The strain measurements recorded at a vehicle speed of 20 m/s for the different moving force cases are presented in Fig. 12.

To determine the optimal window size for the convolution coefficient matrix and improve both accuracy and subspace correctness, this study evaluated various window sizes using the local pseudo force ratio approach, as described in Sect. 2.4.1. A window size of 35 was ultimately selected, as it provided the best results while ensuring the correct subspace. This choice was further validated during the moving force identification process, as shown in Fig. 13. The results demonstrate that a convolution matrix with a

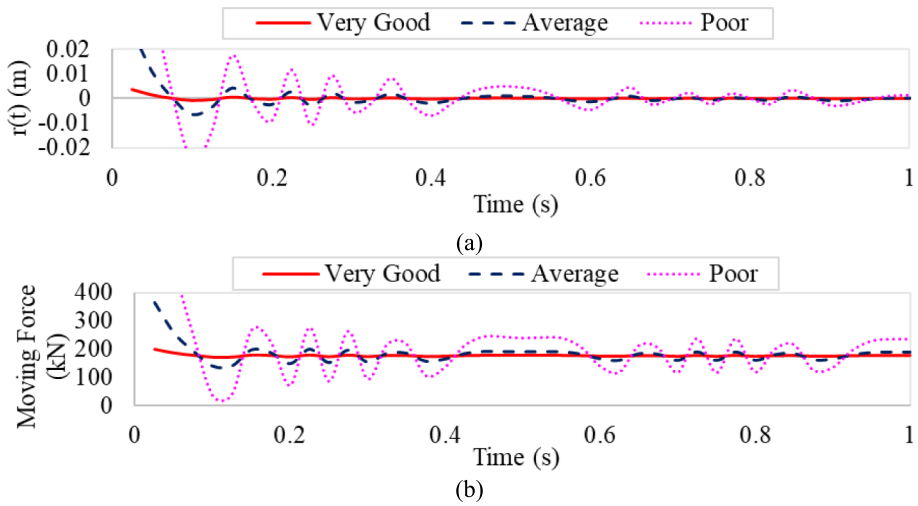


Fig. 11 (**a**) Variation in road surface roughness profile (**b**) variation of moving force under different road surface conditions

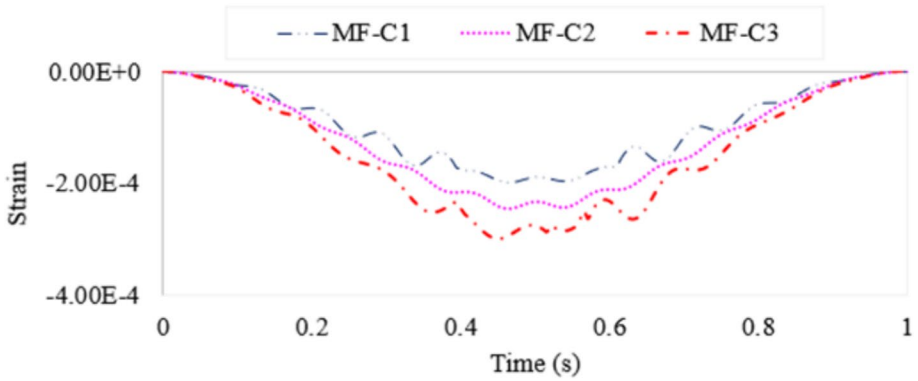


Fig. 12 Strain variation at sensor S-1 for a vehicle speed of 20 m/s on the continuously supported prestressed concrete T-beam

window size of 35 ($\mathbf{C}_{35}$) not only delivers high accuracy in identifying moving forces but also ensures that the subspace of the identified forces closely matches the actual moving forces.

Based on the strain difference responses obtained from different sensor locations in the numerical study and incorporating the convolution matrix ($\mathbf{C}_{35}$), prestress force identification was performed for both levels of prestressing. The prestress force identified using strain difference responses from the sensor pair S1-S2 is shown in Fig. 14.

Additionally, the average identified prestress force, based on strain difference responses from different sensor pairs, is presented in Fig. 15, where it is compared with the actual prestress force at both levels.

To conduct the comparison study on prestress force identification, the relative percentage error (RPE) is calculated using Eq. (30) provided below.

$$\text{RPE} = \frac{||\mathbf{P}_{\text{identified}} - \mathbf{P}_{\text{actual}}||}{||\mathbf{P}_{\text{actual}}||} \times 100\% \tag{30}$$

The RPE was also estimated for both levels of prestressing using strain difference responses obtained from different sensor locations, as tabulated in Table 3. For level 1, the estimated RPE values were 2.66% for sensor pairs S1-S2, 3.23% for S2-S4, 2.53% for S1-S3, 3.15% for S1-S4, and 7.32% for S3-S5. Similarly, for level 2, the estimated RPE values were 1.95%, 4.68%, 2.11%, 3.78%, and 5.68%, respectively. Based on these results, it is confirmed that the proposed method can accurately identify the prestress force with good accuracy and minimal computational effort, as demonstrated by the numerical study.

Furthermore, the study shows that the accuracy of prestress force identification depends on both the sensor location and the selected element length. Accuracy is highest when sensors are placed at or near the mid-span. However, errors increase as sensor

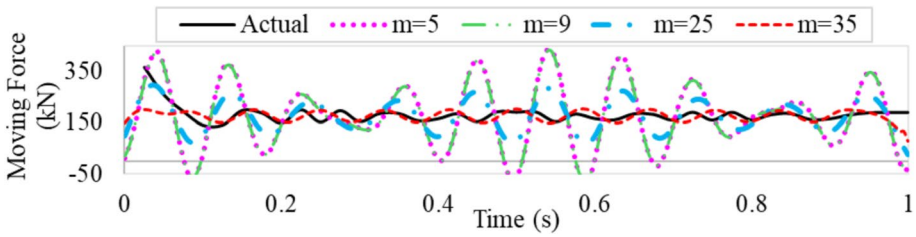


Fig. 13 The moving force identification under different convolution matrices in Case MF-C2 in a continuously supported prestressed concrete T-beam

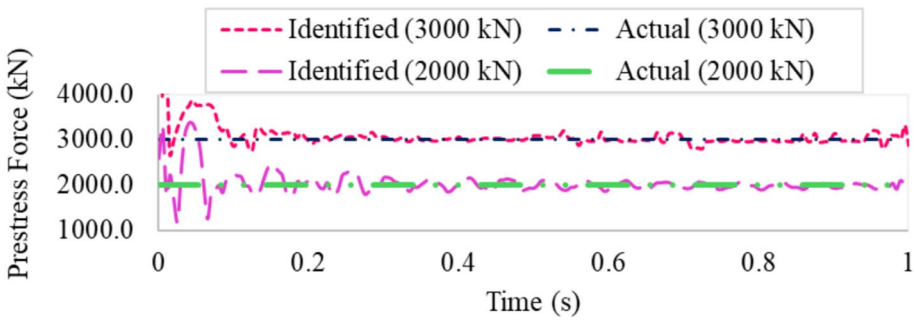


Fig. 14 Prestress force identification using sensor pair S1-S2 in the continuously supported prestressed concrete T-beam

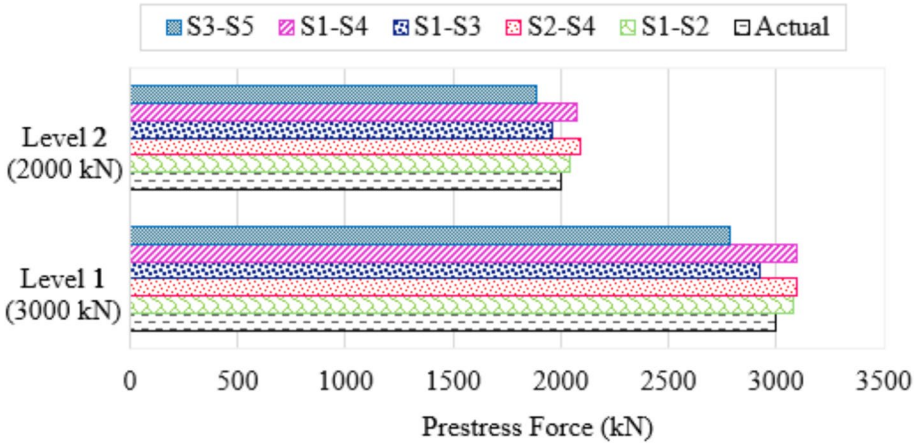


Fig. 15 Average prestress force identified in the continuously supported prestressed concrete T-beam based on strain difference responses from different sensor pairs

Table 3 RPE in prestress force identification using different methods in the continuously supported prestressed concrete T-beam

Sensor location	Stage 1 (3000 kN)	Stage 2 (2000 kN)
S1-S2	2.66	1.95
S2-S4	3.23	4.68
S1-S3	2.53	2.11
S1-S4	3.15	3.78
S3-S5	7.32	5.68

pairs move farther from the mid-span and as the element length increases. Additionally, errors grow when sensor pairs are positioned closer to the supports, as illustrated in Fig. 16.

Additionally, this study identified the moving forces by analysing the strain difference responses for each case and various sensor pairs. The moving forces, determined from the differential strain responses using the dual strain data from sensor pair S1-S2, are shown for cases MF-C1, MF-C2, and MF-C3 in Fig. 17.

Additionally, based on the identified moving forces in the continuously supported prestressed concrete T-beam, the RPE was calculated for all cases and different sensor pairs under different moving force conditions, as shown in Table 4. The RPE for cases MF-C1 through MF-C6 using sensor pairs S1-S2 was 2.15%, 1.20%, 2.52%, 2.08%, 0.75%, and 2.65%, respectively. Similarly, for sensor pairs S2-S4, the RPE was 4.26%, 3.07%, 4.78%, 3.89%, 2.67%, and 4.32%; for S1-S3, it was 2.69%, 0.78%, 2.87%, 2.56%, 0.95%, and 3.03%, for S1-S4, it was 3.87%, 1.98%, 3.68%, 3.01%, 1.91%, and 4.27%, and for S3-S5, it was 5.62%, 4.09%, 6.25%, 4.98%, 3.02%, and 6.99%. Overall, the proposed method demonstrates its capability to accurately identify moving forces in the continuously supported prestressed concrete T-beam.

This study further investigates the influence of sensor locations and element length on the accuracy of moving force identification. Based on the estimated RPE across 30 different conditions involving varying moving forces and sensor pairs, the findings

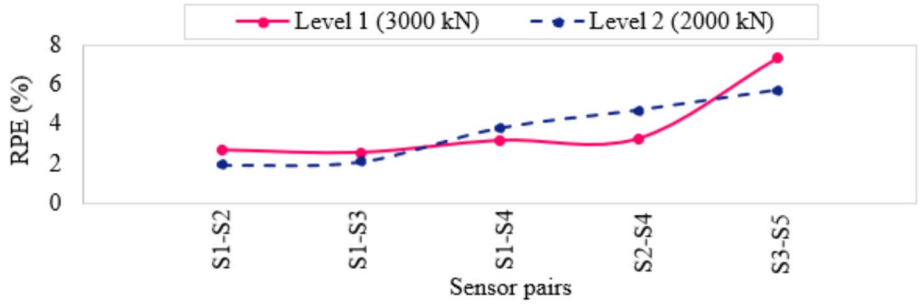


Fig. 16 Variation of the RPE in prestress force identification for a continuously supported prestressed concrete T-beam

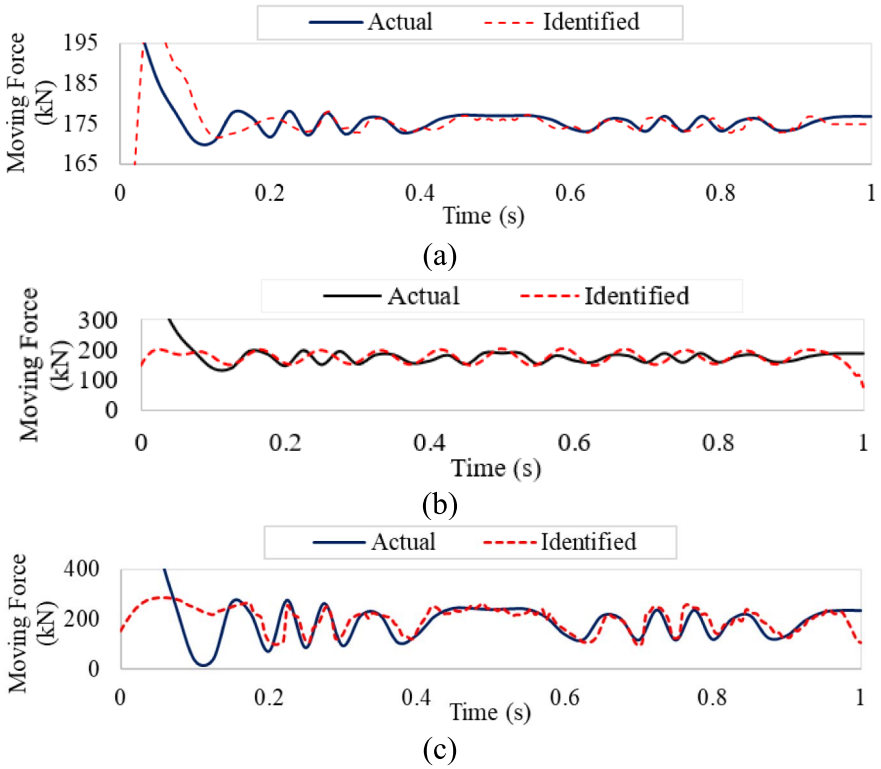


Fig. 17 Moving force identification using sensors S1 and S2 in a continuously supported prestressed concrete T-beam for different cases (**a**) MF-C1 (**b**) MF-C2 (c) MF-C3

Table 4 RPE in moving force identification using different sensor pairs in a continuously supported prestressed concrete T-beam

Cases	RPE (%)				
	S1-S2	S2-S4	S1-S3	S1-S4	S3-S5
MF-C1	2.15	4.26	2.69	3.87	5.62
MF-C2	1.20	3.07	0.78	1.98	4.09
MF-C3	2.52	4.78	2.87	3.68	6.25
MF-C4	2.08	3.89	2.56	3.01	4.98
MF-C5	0.75	2.67	0.95	1.91	3.02
MF-C6	2.65	4.32	3.03	4.27	6.99

suggest that accuracy is higher when sensor pairs and element lengths are positioned near the mid-span compared to when they are placed farther from the mid-span or near the supports. Additionally, accuracy improves when one sensor is located at the mid-span and the other close to it, compared to when the sensors are positioned near the supports, as shown in Fig. 18.

In addition, this study also examines the identification of moving forces in a scenario where two forces travel in opposite directions at a constant speed of 20 m/s, to further demonstrate the capability of the proposed approach. The arrangement of these forces is shown in Fig. 19.

Based on the proposed methodology and the strain responses obtained from the calibrated numerical model, the moving force identification is carried out for the above-mentioned case. The identified moving force results and the variation of the average RPE with the force-spacing-to-span ratio for the considered 1 s time duration are presented in Fig. 20.

Based on the identification results, the two moving forces, F_1 and F_2, were estimated with overall RPEs of 2.46% and 1.88%, respectively. The results indicate that the method maintains good overall accuracy even when the vehicles pass each other. However, as the force-spacing-to-span ratio approaches zero (i.e., two vehicles approach each other), the average local RPE increases and reaches a maximum of approximately 4.85%, as shown in Fig. 20. These findings confirm the capability of the proposed Vandermonde matrix–based convolution procedure to identify moving forces when two vehicles pass each other. By ensuring the correct solution subspace through comparison with the theoretical shape-function ratio derived using a Lagrangian polynomial formulation, the method

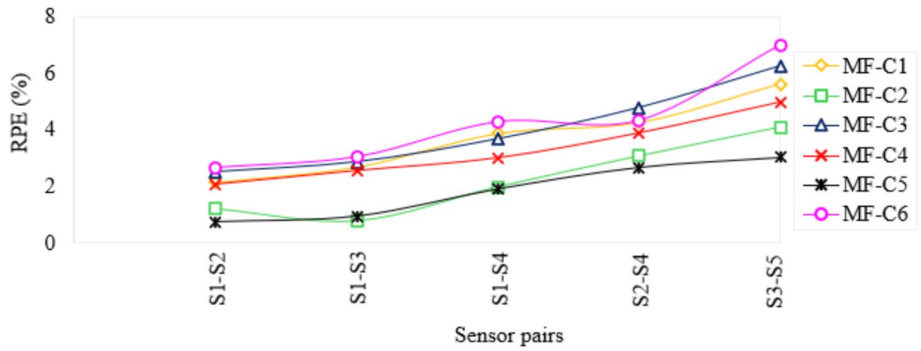


Fig. 18 Variation of the RPE in moving force identification for a continuously supported prestressed concrete T-beam

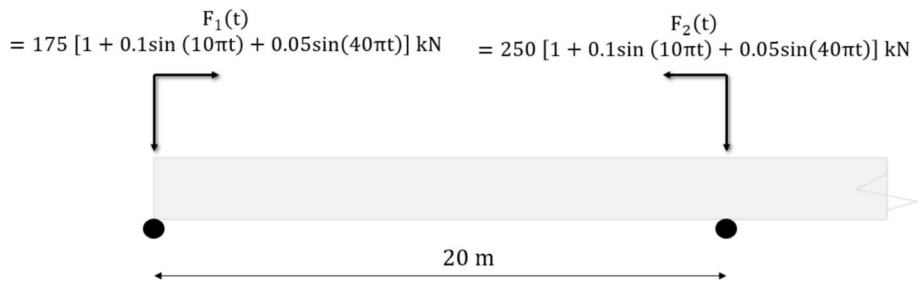


Fig. 19 Two moving-force arrangement on a continuously supported prestressed concrete T-beam

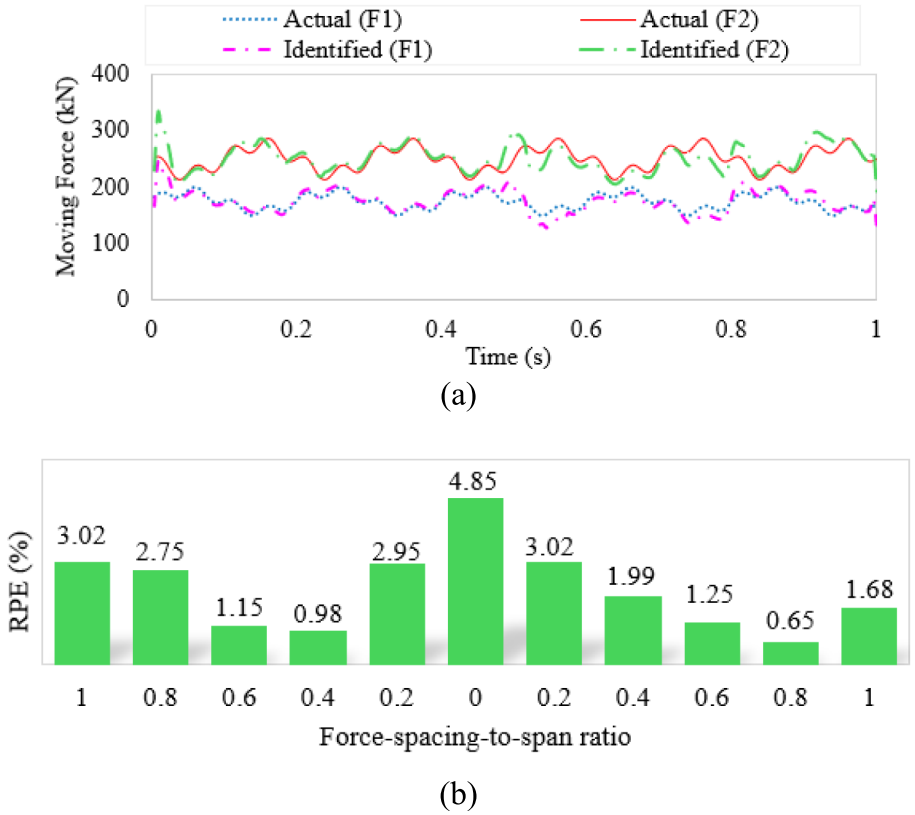


Fig. 20 Comparison of two moving force cases for a continuously supported prestressed concrete T-beam bridge (**a**) identified moving forces for the two cases (**b**) average local RPE of the identified moving forces versus the force-spacing-to-span ratio

enables reliable estimation of each force. Overall, the outcomes demonstrate that the proposed approach can accurately identify two moving forces while correctly capturing their temporal positions in the time-history domain.

In summary, the proposed strain difference response-based approach for identifying prestress and moving forces in a continuously supported prestressed concrete T-beam demonstrates its effectiveness in achieving accurate results while ensuring the correct subspace. Based on the findings on sensor placement, this study recommends positioning sensors at or near the mid-span rather than closer to the supports. This strategy helps minimize computational resources and reduces the burden of handling large amounts of data by focusing on more relevant and effective data.

4 Validation 2: Prestress force and excitation identification in simply supported box-girder bridge model (Experimental study)

4.1 Experimental model of a simply supported prestressed box girder bridge

In this study, a 6-m simply supported prestressed box girder bridge model was used (Pathirage 2017). The Moog control loading system generated excitations at the mid-span of the model. The concrete in the bridge had a density of 2680 kg/m^3 and an elastic modulus of 28.66 GPa. Prestressing forces were applied in three stages with two 15.2 mm diameter unbonded tendons: 171.28 kN (PF1), 284.01 kN (PF2), and 378.29 kN

(PF3). Figure 21 illustrates both the overall view of the bridge model and the experimental setup.

In this study, four strain gauges were used, with their arrangement shown in Fig. 22. Additionally, a modal analysis was conducted at each prestressing stage, and the first three modal frequencies are listed in Table 5.

Additionally, the FE model of the box-girder bridge was developed in Abaqus using a standard explicit model and C3D8R solid elements. Calibration was performed using a model updating technique based on the natural frequencies. The first mode shape for Case PF1 is shown in Fig. 23.

Excitation on the box girder bridge model was applied at the mid-span using the Moog control loading system, which included propulsive force, periodic force, and retarding forces. Strain gauge measurements were taken at a sampling frequency of 1000 Hz, and the variation of applied forces over 1 s is shown in Fig. 24.

To determine the appropriate window size for the simply supported prestressed box girder bridge model, various sensor locations were considered in the FE model, as shown in Fig. 22. The local pseudo force ratio was estimated for each sensor location using the applied convolution matrix, and these results were compared with the theoretical ratio obtained from the shape function approach. The variation of the local pseudo-force ratio at sensor pair S3-S2 is presented in Fig. 25.

Based on the comparison of identification accuracy, as measured by the relative mean square error (RMSE) calculated using Eq. (31), a window size of 25 was selected for the convolution matrix in this study. The variation of RMSE across three cases (S3-S1, S3-S2 and S4-S1) is shown in Fig. 26.

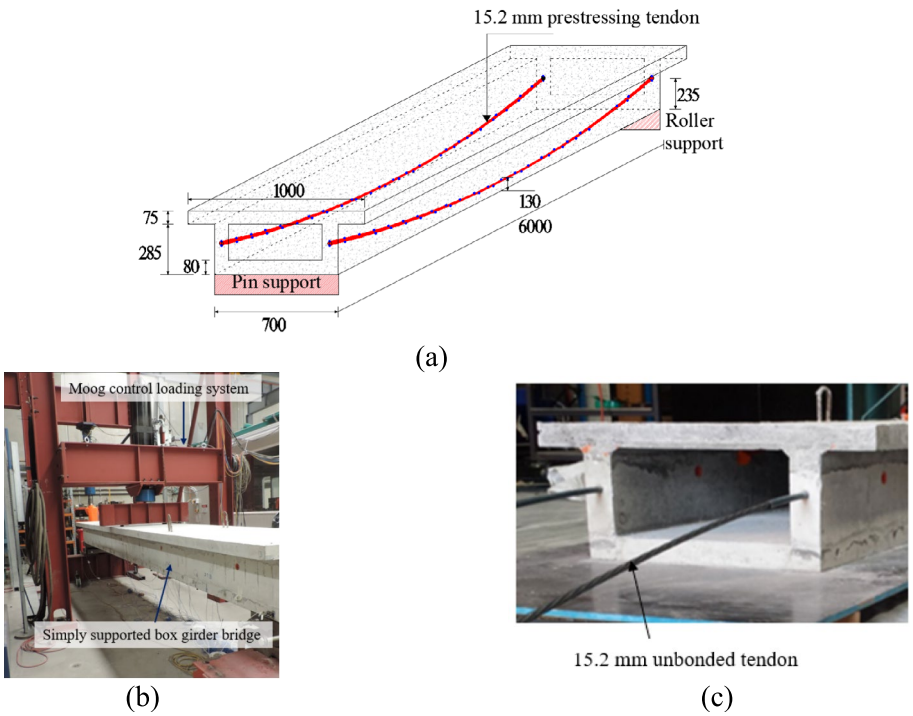


Fig. 21 Simply supported box girder bridge model (**a**) overall view of the bridge model (**b**) experimental bridge model with Moog control loading system (**c**) box girder bridge model with tendon arrangement

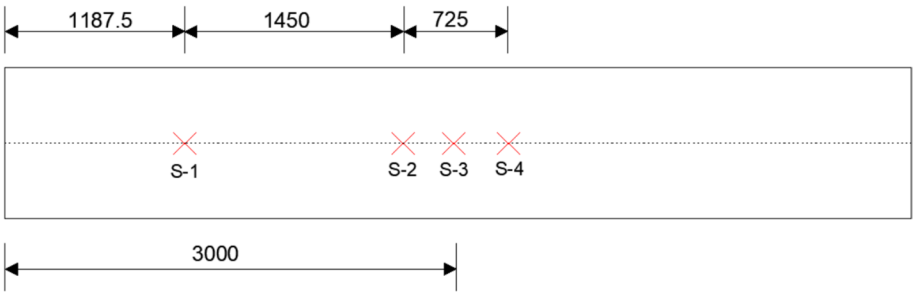


Fig. 22 The placement of the strain gauges in the simply supported box girder bridge model

Table 5 First three natural frequencies at each prestressing stage in the simply supported box-girder bridge model

Cases	PF (kN)	Natural frequency (Hz)		
		Modes		
		1	2	3
PF1	171.28	23.023	43.785	57.768
PF2	284.01	22.973	43.502	57.204
PF3	378.29	22.902	43.536	57.235

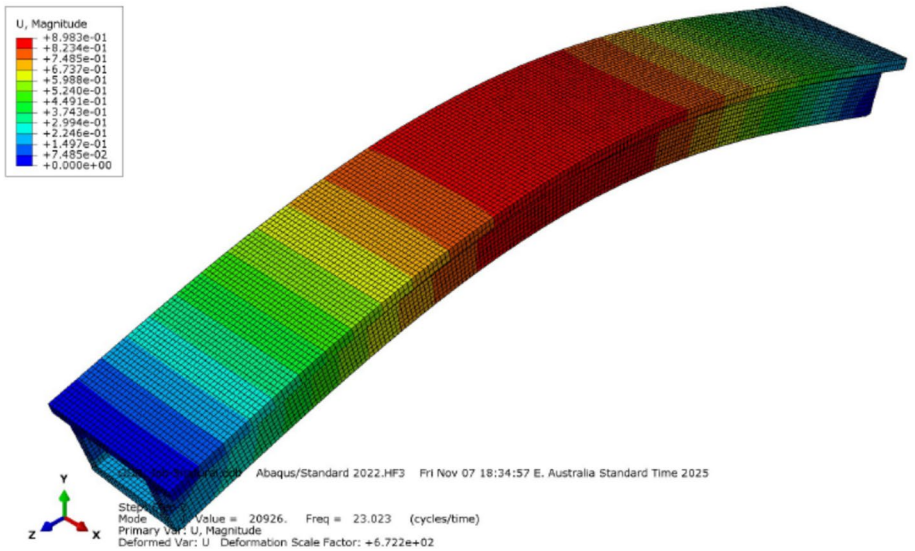


Fig. 23 First mode shape of the simply supported prestressed box-girder bridge model in Case PF1, corresponding to the first natural frequency of 23.023 Hz

$$\mathrm{RMSE}(\%) = 100 * \sqrt{\sum_{i=1}^{n} \frac{(\text{Actual local pseudo force ratio} - \text{estimated local pseudo force ratio})^2}{\text{total number of data}(n)}} \tag{31}$$

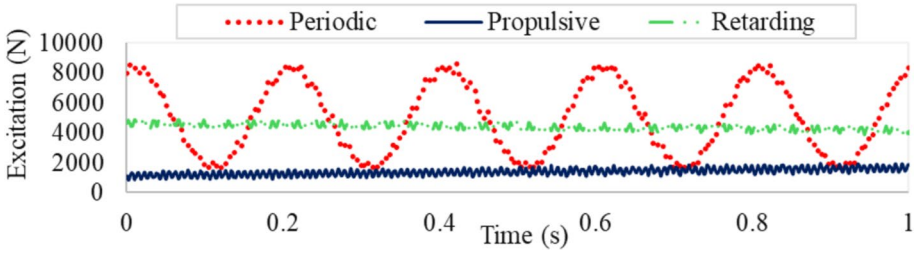


Fig. 24 Excitation at the mid-span of the box-girder bridge model under various loading conditions

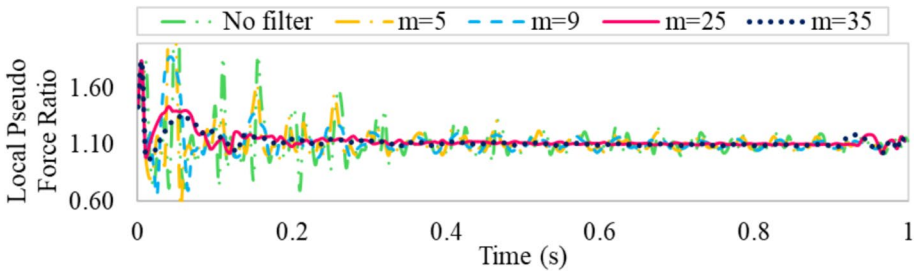


Fig. 25 The variation of the local pseudo force ratio at sensor location S3-S2 under different convolution coefficient matrices

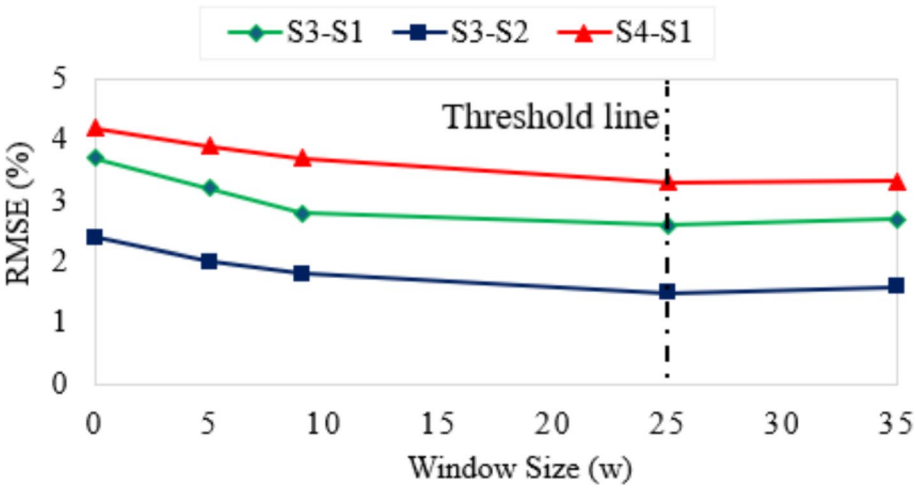


Fig. 26 The variation in RMSE across different window sizes and sensor locations in the simply supported box-girder bridge model

4.2 Prestress force and excitation identification in simply supported box-girder bridge model

To identify the prestress force and moving force, strain measurements obtained under periodic excitation at all four sensor locations in the simply supported prestressed box girder bridge model are presented in Fig. 27 under excitation. Using these strain measurements and incorporating the convolution coefficient matrix ($\mathbf{C}_{25}$) into the prestress force identification methodology, the prestress force is determined based on the relative strain obtained from sensor pairs S3-S2, S3-S1, and S4-S1.

Additionally, the identified prestress force for case PF1, based on the strain difference responses derived from dual strain data over time, is shown in Fig. 28.

Furthermore, the identified average prestress force and RPE for all three cases, based on different sensor pairs, are presented in Fig. 29. Based on the estimated RPE in prestress force identification using strain difference responses, the RPE values for case-PF1 using sensor pairs S3-S2, S3-S1, and S4-S1 are 3.66%, 5.67%, and 7.42%, respectively. In case-PF2, the RPE values are 2.82%, 4.22%, and 6.33%, while in case-PF3, they are 2.20%, 2.57%, and 3.62%, respectively. The experimental study confirms that the proposed method for prestress force identification accurately determines the prestress force using strain difference responses obtained from dual strain measurements along the longitudinal direction of the simply supported box-girder bridge model.

The experimental study on prestress force identification and sensor placement further validates the recommendations made based on the numerical study of a continuously supported prestressed concrete T-beam. It confirms that placing sensors closer to the mid-span yields higher accuracy, while accuracy decreases as sensors are positioned nearer to the supports or as the element length increases.

Additionally, using the convolution coefficient matrix ($\mathbf{C}_{25}$), the vehicle excitation is identified by incorporating strain difference responses from various sensor pairs under different excitation scenarios, including periodic force, propulsive force, and retarding force. The identified excitation force under PF1, using sensors S3-S2, is illustrated in Fig. 30.

Furthermore, the RPE on excitation is estimated for all three prestressing cases, as well as for periodic, propulsive, and retarding excitation scenarios, as shown in Table 6.

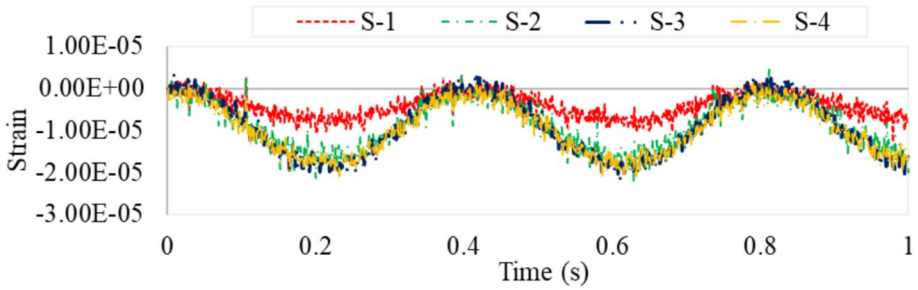


Fig. 27 The variation in strain measurements at different sensor locations in the simply supported prestressed box girder bridge model under excitation

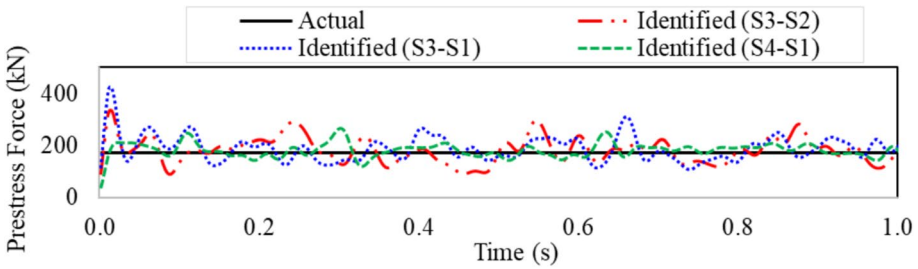


Fig. 28 Identification of prestress force PF1 using strain difference responses in a simply supported box-girder bridge model

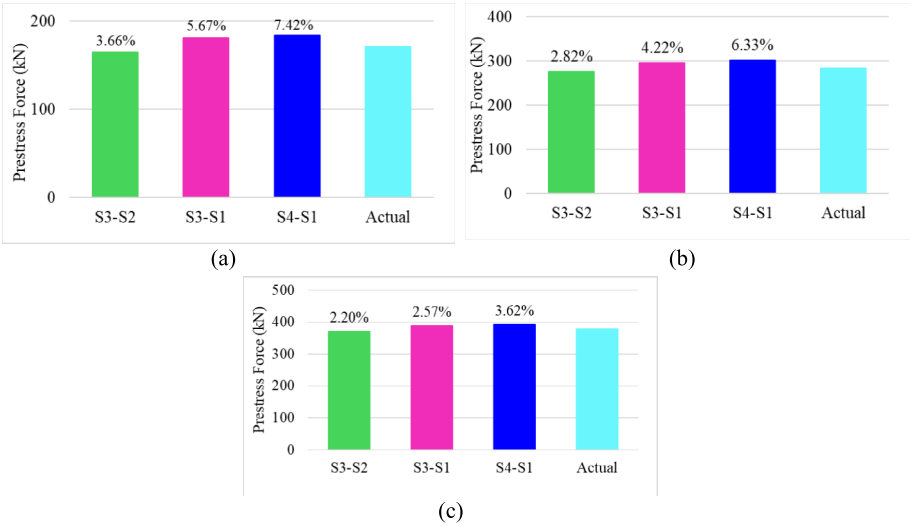


Fig. 29 Identification of prestress force in a simply supported box-girder bridge model using strain difference responses using different sensor pairs (**a**) PF1 (**b**) PF2 (**c**) PF3

The proposed inverse moving force identification method, which incorporates the convolution coefficient matrix to minimize noise, demonstrates its effectiveness by identifying the excitation on the simply supported prestressed box girder bridge model with an RPE of less than 5.02%, while also minimizing computational effort.

In addition to the accuracy of moving force identification, as discussed in the numerical study on a continuously supported prestressed concrete T-beam, sensor pairs positioned closer to the mid-span provide better accuracy compared to those placed farther away. Additionally, increasing the element length gradually reduces accuracy in moving force identification. This recommendation can be further validated by experimental studies under different types of excitations, such as periodic, propulsive, and retarding. As shown in Table 6, the findings confirm that RPE increases for sensor pairs S3-S2, S3-S1, and S4-S1, supporting the statement on sensor placement for moving force identification.

To evaluate the benefits of the proposed method, this study compares it with existing inverse force identification approaches, including the virtual distortion method combined with the load shape function approach (VDM + LSF) (Xiang et al. 2016) and the modified preconditioned conjugate gradient method (M-PCG) (Chen et al. 2018), against the proposed differential strain–based approach. The comparison results for prestress force identification Case 1 (PF1), along with the estimated RPE at 0.2 s time intervals to illustrate the oscillatory behaviour of the results, are presented in Fig. 31.

Based on the time-history behaviour of the identified prestress force and the corresponding RPE variation, it is evident that the proposed differential strain–based approach, combined with the Vandermonde matrix–based convolution process and the incorporation of the pseudo-prestress force concept, significantly improves numerical stability and reduces oscillations in prestress force identification. This results in noticeably higher accuracy compared to existing methods. The VDM + LSF

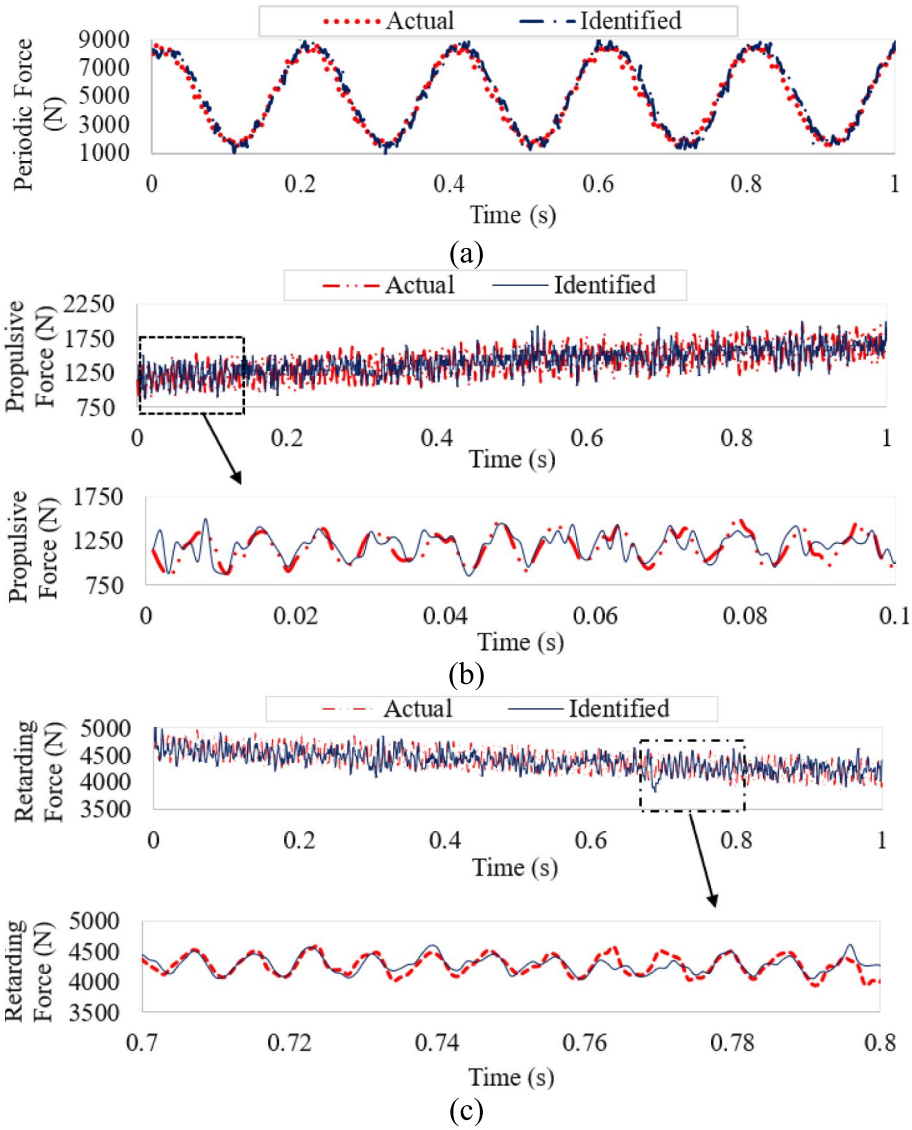
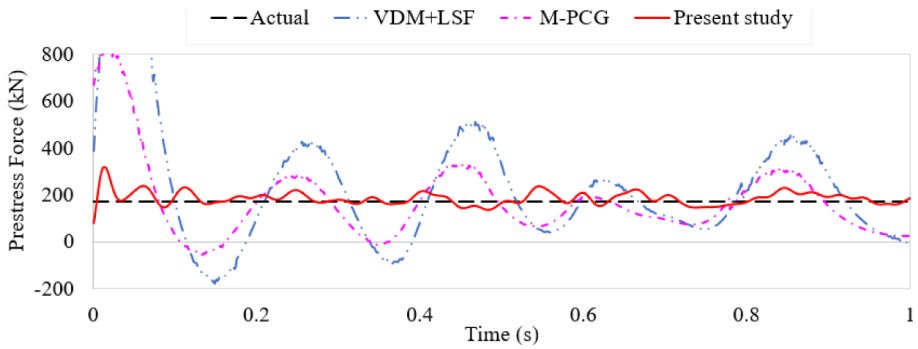


Fig. 30 Identification of excitation using strain difference responses in a simply supported box-girder bridge model (sensor pair S3-S2) in PF1 (**a**) periodic force (**b**) propulsive force (**c**) retarding force

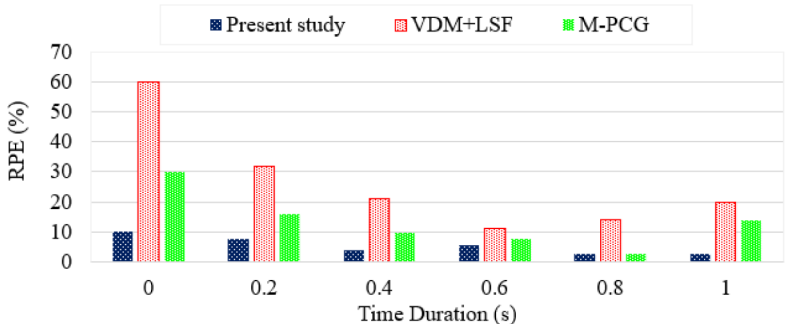
approach shows high sensitivity and produces highly fluctuating identified forces. However, by introducing the pseudo-prestress ratio and Lagrangian polynomial–based shape functions within the convolution framework, the proposed method effectively mitigates instability and achieves higher accuracy. Similarly, although the M-PCG method provides iterative refinement, it requires significantly higher computational effort, especially for real bridges with many elements and many degrees of freedom. The resulting large system matrix increases the number of iterations needed, leading to higher computational demand. Moreover, the M-PCG method still exhibits greater oscillation in the identified forces compared to the proposed approach. In contrast, the present method achieves more stable and accurate identification using a simplified convolution process while ensuring the correct subspace through the local

Table 6 The RPE in the identified excitation for a simply supported box girder bridge under various prestress forces and loading conditions

Cases	Excitation type	RPE (%)		
		S3-S2	S3-S1	S4-S1
E1-PF1	Periodic	2.85	3.24	4.89
E2-PF1	Propulsive	1.92	3.03	4.25
E3-PF1	Retarding	0.58	1.98	2.23
E1-PF2	Periodic	2.45	3.02	3.92
E2-PF2	Propulsive	3.25	3.42	4.05
E2-PF2	Retarding	1.65	3.12	5.02
E1-PF3	Periodic	2.12	2.65	2.99
E2-PF3	Propulsive	1.08	2.23	3.75
E3-PF3	Retarding	1.98	2.25	3.13



The time-history behaviour of the identified prestress force



RPE variation over 0.2 s time intervals

Fig. 31 Prestress force identification in the simply supported box girder bridge model for Case 1 (PF1), comparing the VDM + LSF approach, the M-PCG method, and the proposed method

pseudo-prestress concept. Therefore, the results clearly demonstrate that the proposed approach can deliver accurate and stable prestress force identification using only two strain measurements, outperforming both the VDM + LSF and M-PCG methods.

Additionally, the proposed approach relies on dual strain responses, which reduces the required data volume for effective force identification. In contrast, displacement-based

methods, such as the VDM combined with the LSF approach, require both displacement and rotational measurements because translational and rotational degrees of freedom must be considered in constructing the system matrix. This substantially increases the measurement effort, instrumentation requirements, and processing time.

Ultimately, the proposed differential strain-based method for prestress and moving force identification, incorporating the convolution matrix, demonstrates its ability to accurately identify both forces while ensuring the correct subspace. This is supported by numerical studies on a continuously supported prestressed concrete T-beam, as well as experimental studies on a simply supported box-girder bridge model. Additionally, both the experimental and numerical studies validate that placing sensors closer to the mid-span and reducing the sensor spacing (element length) results in higher accuracy compared to sensor placements near the supports.

5 Validation 3: Prestress and moving force identification in real three-span continuously supported PCBs (Real bridge monitoring data and Numerical study)

5.1 Identification of moving forces in real, continuously supported three-span PCBs using dual strain data

A three-span continuously supported PCB bridge with spans of 99 m, 180 m, and 99 m, respectively, with a total length of 378 m is used to validate the proposed method. Strain responses on this bridge were measured using electrical resistance strain gauges installed at sensor locations S1 and S2 (both placed on the soffit on the left side of the top slab). In addition, a magnetic accelerometer positioned at mid-span (sensor location S1 on the left side of the bottom slab) was used to measure acceleration responses. Acceleration measurements were utilized in this study to extract modal parameters under vehicle movement, validate the FE model, and confirm the vehicle entrance time on the PCB. Figure 32 illustrates the bridge's longitudinal and cross-sectional views with sensor locations (S1 and S2), as well as the FE model constructed using the Abaqus standard explicit approach.

Based on the available data, this study considered six different vehicle categories derived from the dynamic weighing data (09th September 2023, from 12.00 AM to 6.00 AM), and the respective vehicle weights and speeds were extracted as shown in Fig. 33.

Acceleration responses from a magnetic accelerometer placed at mid-span (sensor location S1) were used to extract the modal frequencies and validate the FE model, ensuring it accurately reflects the structural performance of the real PCB. From the modal analysis, the first three modal frequencies were determined to be 0.95 Hz, 2.12 Hz, and 2.78 Hz, respectively. Model updating was then performed, resulting in a maximum error of 4.25%, and further verified by comparing the measured bending strain with the overall static weight obtained from the B-WIM system. Following model updating, the concrete density was set to 2650 kg/m^3, the elastic modulus to 35.55 GPa, and the Poisson's ratio to 0.2. All sensors are sampled at a frequency of 10 Hz. Figure 34 illustrates the time-domain and frequency-domain acceleration responses under vehicle movement.

To validate the proposed dual strain-based approach for moving force identification, this study examines six different vehicle types and records their strain responses without

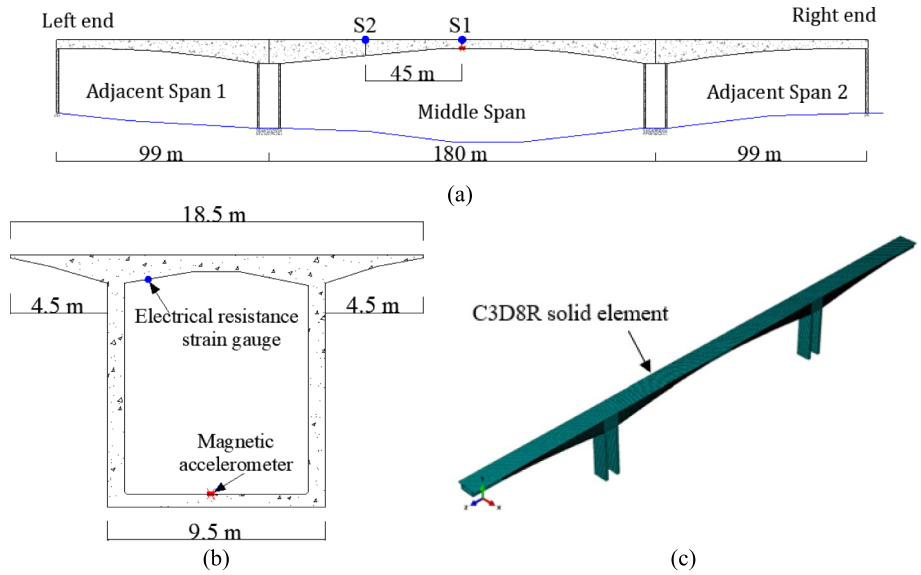


Fig. 32 Real three-span continuously supported PCBs information (**a**) longitudinal view of the bridge and sensor location (**b**) cross-section view with sensor location (**c**) FE 3D mesh view

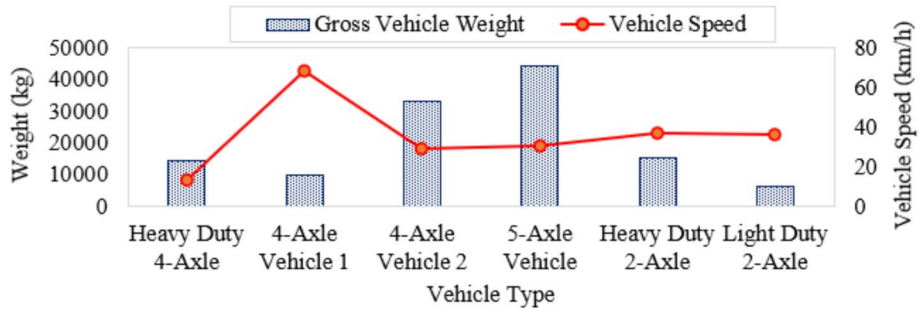


Fig. 33 Different vehicle types, along with their respective weights and speeds on the three-span, continuously supported PCBs at different times, based on dynamic weighing data

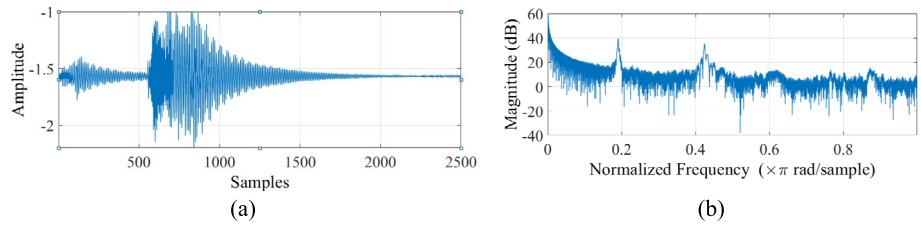


Fig. 34 Acceleration responses obtained at sensor location at S1 (mid-span) of the 3-span continuously supported PCBs under vehicle movement (**a**) time domain (**b**) frequency domain

prior knowledge of any vehicle-related information. The strain responses obtained at mid-span for each vehicle type are presented in Fig. 35.

As previously described, the prestressed bridge-vehicle system matrix is constructed using a calibrated FE model. Strain responses are derived from the difference between the signals at S1 and S2. To ensure accuracy and determine the correct subspace, a convolution matrix with a window size of 25 ($\mathbf{C}_{25}$) is created based on

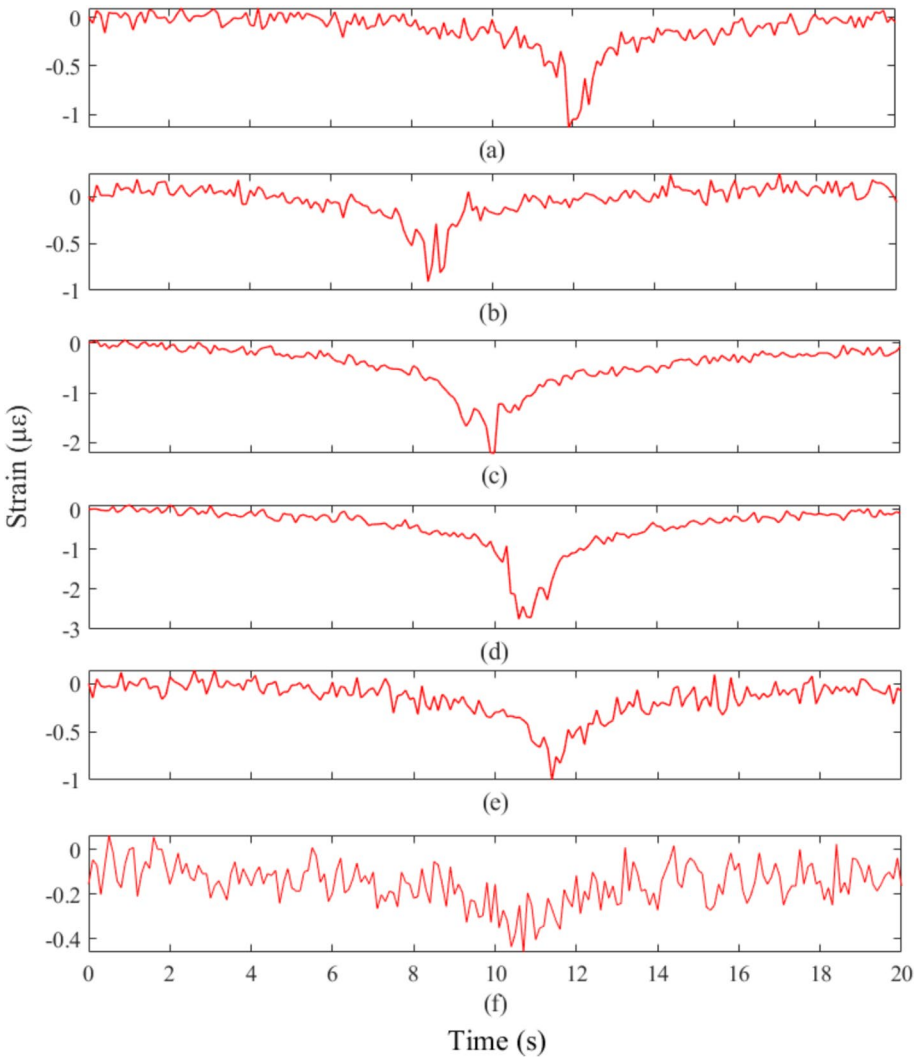


Fig. 35 Strain responses obtained at sensor location at S1 (mid-span) of the 3-span continuously supported PCBs under different vehicles (**a**) heavy-duty 4-axle (**b**) 4-axle vehicle 1 (**c**) 4-axle vehicle 2 (**d**) 5-axle vehicle (**e**) heavy-duty 2-axle (**f**) light duty 2-axle

dynamic weighing data. Consequently, the strain responses from the S1–S2 sensor pair are used to identify the moving forces, which are then compared with the equivalent gross vehicle weight obtained from dynamic weighing data measured at the stable position on the road near the left end of the PCB, as illustrated in Fig. 36.

To evaluate the robustness of the moving force identification, the average identified moving forces are compared with the equivalent gross weight of each vehicle, and the RPEs are estimated, as illustrated in Fig. 37.

Based on the estimated RPEs, the proposed dual-strain-based approach—combined with a regularization technique that incorporates a convolution matrix derived from the Vandermonde matrix demonstrates its effectiveness in accurately identifying moving forces in real-world PCBs and could be used as a simple but effective B-WIM system.

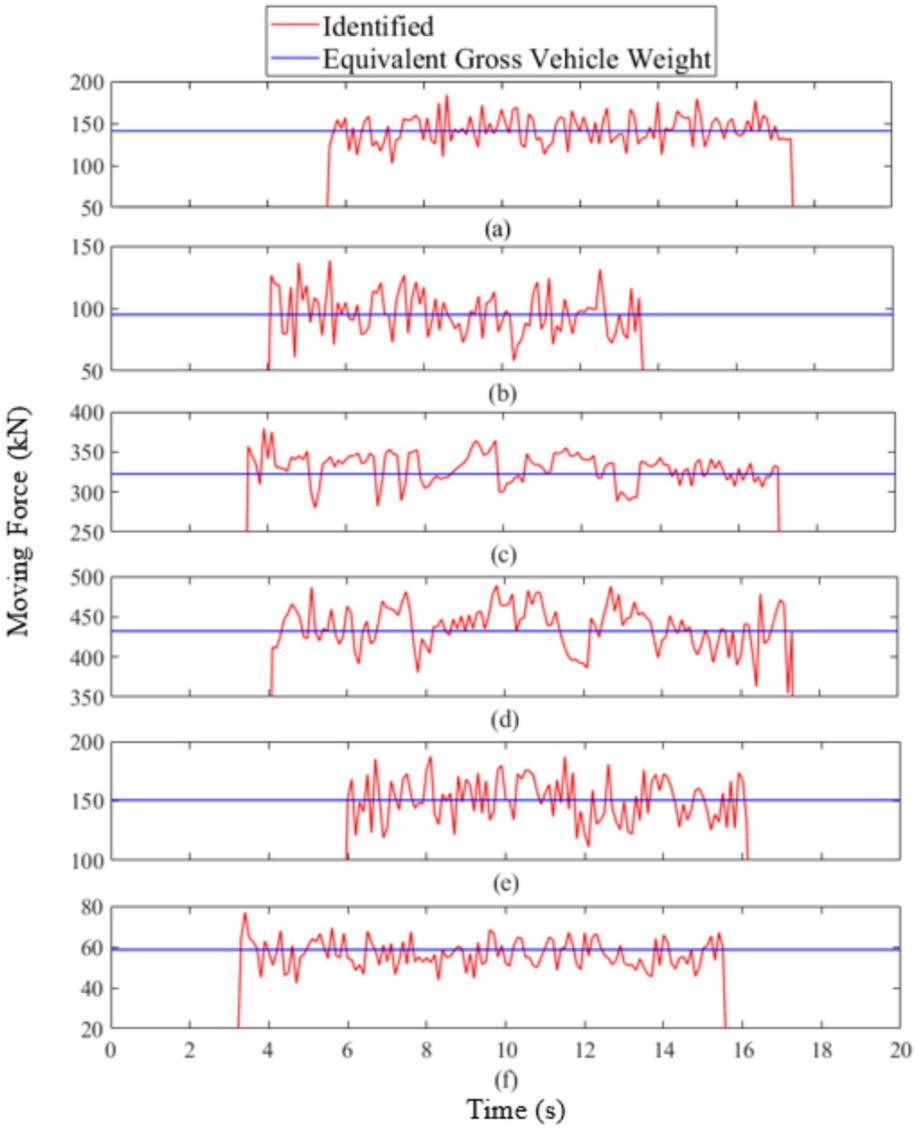


Fig. 36 Identified moving forces using differential strain responses from sensor pair S1–S2 for different vehicles in a 3-span continuously supported PCB (**a**) heavy-duty 4-axle (**b**) 4-axle vehicle 1 (**c**) 4-axle vehicle 2 (**d**) 5-axle vehicle (**e**) heavy-duty 2-axle (**f**) light duty 2-axle

5.2 Identification of prestress forces in real, continuously supported three-span PCBs through a numerical study

In the real bridge, prestressing was carried out using 15.2 mm tendons with a breaking strength of 1860 MPa. The maximum design limit factor was 0.75. To simulate the strain responses at sensor locations S1 and S2 for validating the proposed prestress force identification method, a calibrated FE model of the three-span continuously supported PCB was used. Three different levels of prestressing {initial (16,790 kN), Level 1 (11,750 kN), and Level 2 (7,500 kN)} were introduced using a load-balancing technique to generate the strain responses required for validating the dual strain-based approach. The tendon profile arrangement is shown in Fig. 38.

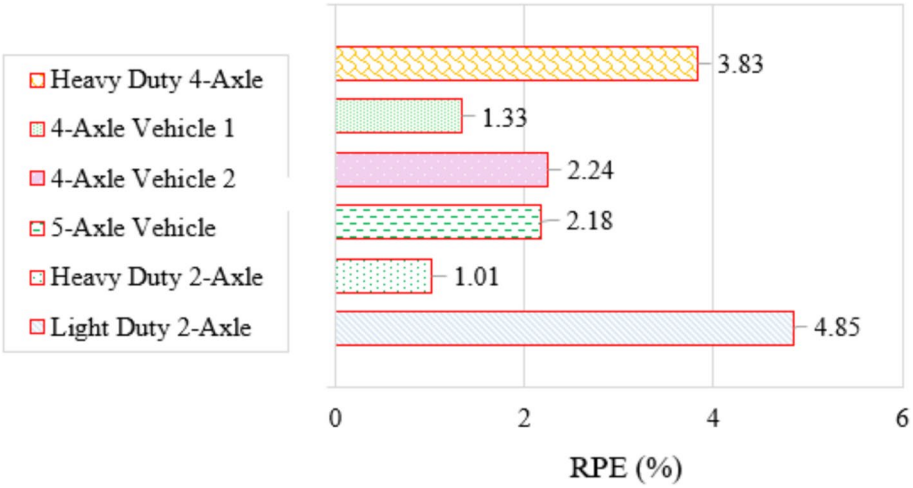


Fig. 37 Estimated RPE for various vehicle types used in moving force identification on a real, continuously supported, three-span PCB

The tendon profile has an eccentricity of 2400 mm at the convex area and 600 mm at the concave area. Under random excitation, strain responses are simulated at sensor locations S1 and S2 for two different levels of prestressing. These responses are then used to identify the prestress forces, following the methodology described in Sect. 2.2. By analysing the differential strain derived from dual strain data, the prestress force is identified in all three levels and then compared with the actual prestress force, as illustrated in Fig. 39.

Based on the estimated RPE for prestress force identification (compared to actual values), the RPE values are 6.89%, 3.48% and 2.96% for prestressing initial, level 1 and level 2, respectively. These results demonstrate the method's effectiveness in accurately identifying prestress forces in continuously supported PCBs.

In summary, beyond the numerical and experimental studies, the proposed dual-strain-based approach effectively ensures accurate identification of both moving and prestress forces in real PCBs, while requiring minimal computational resources and effort. Compared to existing methods—which rely directly on strain responses that suffer from high ill-posedness when applied to real bridge cases due to the high sensitivity of sensor measurements to external factors—the proposed differential strain-based approach overcomes these challenges. It significantly improves the accuracy and efficiency of prestress and moving force identification. The results presented provide strong evidence of this advancement. The strain measurements from the electrical resistance

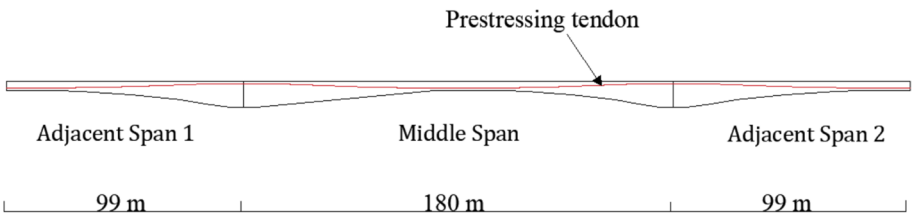


Fig. 38 Arrangement of prestressing tendons in the three-span, continuously supported PCB

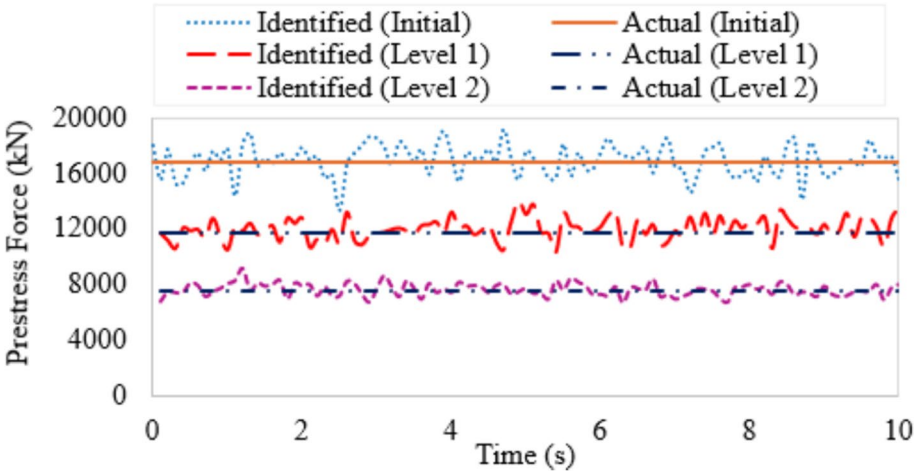


Fig. 39 Comparison between the identified and actual prestress forces in a three-span, continuously supported PCB, incorporating different prestress levels based on the FE model

strain gauge at sensor location S1, along with the refined strain data obtained using the selected convolution matrix as discussed in the validation section, are presented in Fig. 40. This ensures that only the useful features of the strain response are extracted for effective moving force identification.

Based on the above figure, the effects of uncertainties on the strain input are evident, highlighting the effectiveness of the proposed method in overcoming these challenges. By minimizing the impact of uncertainties, the proposed approach reduces the burden on bridge managers, enabling accurate and efficient identification of prestress and moving forces using only dual strain responses. This, in turn, supports timely decisions regarding bridge serviceability and helps safeguard bridge users.

6 Conclusions

A novel differential strain-based approach has been developed for identifying prestress and moving forces, incorporating a convolution matrix. The convolution matrix, developed using a Vandermonde matrix, is designed to effectively reduce noise by regularizing the inverse problem, allowing for a least-squares solution while preserving the correct subspace. Notably, it requires only dual strain responses along the longitudinal direction of PCBs to achieve accurate results. The study also presents the pseudo-prestress

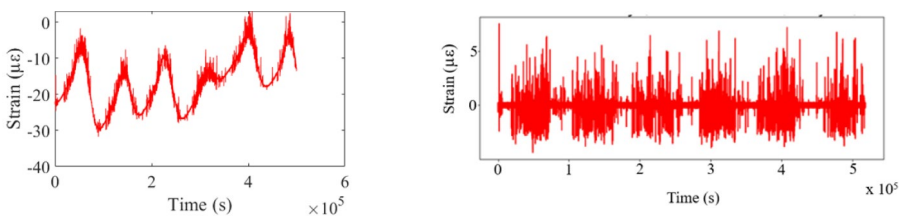


Fig. 40 Time-history of electrical resistance strain gauge data and refined strain data under moving vehicle conditions on the three-span real PCB

force ratio to determine the optimal window size for the convolution matrix, reducing computational effort. The proposed methodology was validated through experimental data from a simply supported prestressed box-girder bridge model, which included three stages of prestressing and three types of excitations: propulsive, periodic, and retarding. Further verification was performed using a continuously supported prestressed concrete T-beam with two stages of prestressing, subjected to varying moving forces under different bridge surface conditions and vehicle speeds. In addition to experimental and numerical studies, the proposed method is applied to real, three-span, continuously supported PCBs using actual strain and dynamic weighing data to ensure its robustness. Based on this study the following conclusions can be drawn:

i. The proposed approach not only enables accurate and efficient identification of prestress and moving forces but also demonstrates the potential of a smart sensing strategy by utilizing just dual strain responses through a differential strain-based method.
ii. The proposed time-domain based inverse prestress and moving force identification approach demonstrates strong capability in identifying both prestress and moving forces with improved numerical stability and higher accuracy compared to existing methods.
iii. This study provides strategic guidelines for optimal sensor placement along the longitudinal axis of PCBs, enabling effective identification of prestress and moving forces with minimal sensor deployment and reduced computational demand. Validated by both numerical and experimental investigations, the results reveal that positioning sensors closer to the mid-span significantly enhances accuracy, with performance progressively improving as sensors are moved away from the supports toward the mid-span.
iv. The proposed effective approach enables bridge managers to extend the service life of real-world PCBs through timely maintenance. Furthermore, by relying on strain measurements, the proposed method eases the burden of sensor installation and monitoring, reducing both inconvenience and operational challenges.

This study focused on developing an enhanced approach for identifying prestress and moving forces using differential strain derived from dual strain responses. While the proposed method has demonstrated its applicability to both simply supported and continuously supported PCBs, it is currently limited to overall axle force identification. Future research will extend this methodology to identify prestress and moving forces in deep girders and wide box-girder bridges by explicitly incorporating shear deformation and torsional effects. In addition, the method will be further evaluated for vehicle crossing scenarios through experimental studies and instrumented field testing. In addition, long-term continuous monitoring data will be utilized to further validate the accuracy of the prestress force identification. The benchmark prestress values will be estimated using standard prestress-loss calculation formulas to enable direct comparison and to further establish the engineering value of the proposed method.

Acknowledgements
The authors also would like to acknowledge Dr. Ziru Xiang for providing the experimental data and other assistance to conduct this research.

Authors' contributions
K J: Conceptualization, Design of the study, Methodology, Data analysis, Visualization, Software, Writing-original draft. T C: Supervision, Design of study, Writing-review & editing, Funding acquisition, Project administration. K N: Supervision, Design of the study, Writing-review & editing, and Funding acquisition. D P: Supervision, Writing-review & editing. X Z: Data curation, Design of study, Funding acquisition, Writing-review & editing. D W and E Z: Data curation.

Funding
This research is part of a Discovery Project funded by the Australian Research Council (ARC), "Next Generation Bridge Monitoring using Novel Synergic Identification" (DP220102045). The third author would like to acknowledge the financial support from the ARC DECRA award DE220100909.

Data availability
The datasets used and/or analysed during the current study are available from the corresponding author on reasonable request.

Declarations

Competing interests
Xinqun Zhu is an editorial board member for Advances in Bridge Engineering and was not involved in the editorial review, or the decision to publish, this article. The authors declare that they have no known competing financial interests or personal relationships that could have appeared to influence the work reported in this paper.

Received: 6 January 2026 Revised: 19 February 2026 Accepted: 3 March 2026
Published online: 02 July 2026

References

Acharya D, Rani A, Agarwal S, Singh V (2016) Application of adaptive Savitzky-Golay filter for EEG signal processing. Perspect Sci (Neth) 8:677–679. https://doi.org/10.1016/j.pisc.2016.06.056
Agostinacchio M, Ciampa D, Olita S (2014) The vibrations induced by surface irregularities in road pavements – a Matlab® approach. Eur Transp Res Rev 6:267–275. https://doi.org/10.1007/s12544-013-0127-8
Bagge N, Nilimaa J, Elfgren L (2017) In-situ methods to determine residual prestress forces in concrete bridges. Eng Struct 135:41–52. https://doi.org/10.1016/j.engstruct.2016.12.059
Biswal S, Ramaswamy A (2016) Measurement of existing prestressing force in concrete structures through an embedded vibrating beam strain gauge. Measurement 83:10–19. https://doi.org/10.1016/j.measurement.2016.01.031
Bonopera M, Chang K-C, Lee Z-K (2020) State-of-the-Art review on determining prestress losses in prestressed concrete girders. Appl Sci 10:7257. https://doi.org/10.3390/app10207257
Breccolotti M (2020) Eigenfrequencies of continuous prestressed concrete bridges subjected to prestress losses. Structures 25:138–146. https://doi.org/10.1016/j.istruc.2020.03.011
Cao D, Qin X-C, Meng S-P, Tu Y-M, Elfgren L, Sabourova N, Grip N, Ohlsson U, Blanksvärd T (2016) Evaluation of prestress losses in prestressed concrete specimens subjected to freeze–thaw cycles. Struct Infrastruct Eng 12:159–170. https://doi.org/10.1080/15732479.2014.998241
Chan THT, Yung TH (2000) A theoretical study of force identification using prestressed concrete bridges. Eng Struct 22:1529–1537. https://doi.org/10.1016/S0141-0296(99)00087-5
Chan THT, Law SS, Yung TH (2000) Moving force identification using an existing prestressed concrete bridge. Eng Struct 22:1261–1270. https://doi.org/10.1016/S0141-0296(99)00084-X
Chan THT, Yu L, Law SS, Yung TH (2001a) Moving force identification studies, I: theory. J Sound Vib 247:59–76. https://doi.org/10.1006/jsvi.2001.3630
Chan THT, Yu L, Law SS, Yung TH (2001b) Moving force identification studies, II: comparative studies. J Sound Vib 247:77–95. https://doi.org/10.1006/jsvi.2001.3629
Chávez AA, Gonzalez-Libreros J, Wang C, Capacci L, Biondini F, Elfgren L, Sas G (2024) Assessment of residual prestress in existing concrete bridges: the Kalix bridge. Eng Struct 311:118194. https://doi.org/10.1016/j.engstruct.2024.118194
Chen Z, Chan THT, Nguyen A (2018) Moving force identification based on modified preconditioned conjugate gradient method. J Sound Vib 423:100–117. https://doi.org/10.1016/j.jsv.2017.11.034
Chen Z, Chan THT, Yu L (2020) Comparison of regularization methods for moving force identification with ill-posed problems. J Sound Vib 478:115349. https://doi.org/10.1016/j.jsv.2020.115349
Chen Z, Sun P, Chan THT, Yu L (2021) Ill-posedness determination of moving force identification and parameters selection for regularization methods. Int J Struct Stab Dyn 21:2150114. https://doi.org/10.1142/S0219455421501145
Chen Z, Deng L, Kong X (2022) Modified truncated singular value decomposition method for moving force identification. Adv Struct Eng 25:2609–2623. https://doi.org/10.1177/13694332221104278
Ho D-D, Kim J-T, Stubbs N, Park W-S (2012) Prestress-force estimation in PSC girder using modal parameters and system identification. Adv Struct Eng 15:997–1012. https://doi.org/10.1260/1369-4332.15.6.997
Hussin M, Chan THT, Fawzia S, Ghasemi N (2020) Identifying the prestress force in prestressed concrete bridges using ultrasonic technology. Int J Struct Stab Dyn 20:2042014. https://doi.org/10.1142/S0219455420420146

Jeyamohan K, Chan THT, Nguyen K-D, Thambiratnam DP (2024) Prestress force and moving force identification in prestressed concrete bridges via Lagrangian polynomial-based load shape function approach. J Civ Struct Health Monit. https://doi.org/10.1007/s13349-024-00822-9
Jeyamohan K, Chan THT, Nguyen K-D, Thambiratnam DP, Zhu X (2025) Internal force identification in prestressed concrete bridges via Lagrangian interpolation and substructural modelling technique. Int J Struct Stab Dyn. https://doi.org/10.1142/S021945542640002X
Jia S, Akiyama M, Han B, Frangopol DM (2023) Probabilistic structural identification and condition assessment of prestressed concrete bridges based on Bayesian inference using deflection measurements. Structure and Infrastructure Engineering 1–17. https://doi.org/10.1080/15732479.2023.2192508
Khandel O, Soliman M, Floyd RW, Murray CD (2021) Performance assessment of prestressed concrete bridge girders using fiber optic sensors and artificial neural networks. Struct Infrastruct Eng 17:605–619. https://doi.org/10.1080/15732479.2020.1759658
Kim J-M, Kim H-W, Park Y-H, Yang I-H, Kim Y-S (2012) FBG sensors encapsulated into 7-Wire steel strand for tension monitoring of a prestressing tendon. Adv Struct Eng 15:907–917. https://doi.org/10.1260/1369-4332.15.6.907
Kralovanec J, Bahleda F, Moravcik M (2022) State of prestressing analysis of 62-year-old bridge. Materials 15:3583. https://doi.org/10.3390/ma15103583
Lai X, Furkan M, Bartoli I, Aktan AE, Grimmelsman K (2022) Bridge weigh-in-motion using augmented Kalman filter and model updating. J Civ Struct Health Monit 12:593–610. https://doi.org/10.1007/s13349-022-00559-3
Law SS, Lu ZR (2005) Time domain responses of a prestressed beam and prestress identification. J Sound Vib 288:1011–1025. https://doi.org/10.1016/j.jsv.2005.01.045
Law SS, Chan THT, Zeng QH (1997) Moving Force Identification: a time domain method. J Sound Vib 201:1–22. https://doi.org/10.1006/jsvi.1996.0774
Law SS, Chan THT, Zeng QH (1999) Moving Force Identification—a frequency and time domains analysis. J Dyn Syst Meas Control 121:394–401. https://doi.org/10.1115/1.2802487
Lu ZR, Law SS (2006) Identification of prestress force from measured structural responses. Mech Syst Signal Process 20:2186–2199. https://doi.org/10.1016/j.ymssp.2005.09.001
Luo J, Ying K, He P, Bai J (2005) Properties of Savitzky-Golay digital differentiators. Digit Signal Process 15:122–136. https://doi.org/10.1016/j.dsp.2004.09.008
Ma L, Zhang W, Han WS, Liu JX (2019) Determining the dynamic amplification factor of multi-span continuous box girder bridges in highways using vehicle-bridge interaction analyses. Eng Struct 181:47–59. https://doi.org/10.1016/j.engstruct.2018.11.059
Ma Z, Choi J, Sohn H (2023) Structural displacement sensing techniques for civil infrastructure: a review. J Infrastruct Intell Resil 2:100041. https://doi.org/10.1016/j.iintel.2023.100041
Páez PM (2023) A simplified approach to determine the prestress loss and time-dependent deflection in cracked prestressed concrete members, prestressed with fiber reinforced polymers or steel tendons. Eng Struct 279:115523. https://doi.org/10.1016/j.engstruct.2022.115523
Pathirage TS (2017) Identification of prestress force in prestressed concrete box girder bridges using vibration based techniques. PhD thesis, Queensland University of Technology. https://doi.org/10.5204/thesis.eprints.112767
Rahman MdH, Gupta C (2020) Computation of Rayleigh damping coefficient of a rectangular submerged floating tunnel (SFT). SN Appl Sci 2:936. https://doi.org/10.1007/s42452-020-2629-z
Rashetnia R, Ghasemzadeh F, Hallaji M, Pour-Ghaz M (2018) Quantifying prestressing force loss due to corrosion from dynamic structural response. J Sound Vib 433:129–137. https://doi.org/10.1016/j.jsv.2018.07.012
Saiidi M, Douglas B, Feng S (1994) Prestress force effect on vibration frequency of concrete bridges. J Struct Eng 120:2233–2241. https://doi.org/10.1061/(ASCE)0733-9445(1994)120:7(2233)
Savitzky A, Golay MJE (1964) Smoothing and differentiation of data by simplified least squares procedures. Anal Chem 36:1627–1639. https://doi.org/10.1021/ac60214a047
Staggs JEJ (2005) Savitzky-Golay smoothing and numerical differentiation of cone calorimeter mass data. Fire Saf J 40:493–505. https://doi.org/10.1016/j.firesaf.2005.05.002
Talaei S, Zhu X, Li J, Yu Y, Chan THT (2025) A hybrid domain adaptation approach for estimation of prestressed forces in prestressed concrete bridges under moving vehicles. Eng Struct 330:119904. https://doi.org/10.1016/j.engstruct.2025.119904
Tse FS, Morse IE, Hinkle RT (1978) Mechanical vibrations, theory and applications. Allyn and Bacon, Inc, Boston
Van Breugel FV, Kutz JN, Brunton BW (2020) Numerical differentiation of noisy data: a unifying multi-objective optimization framework. IEEE Access 8:196865–196877. https://doi.org/10.1109/ACCESS.2020.3034077
Van Van L, Thanh Tung N (2023) Influence of road quality and suspension stiffness on passenger vehicles oscillation in Viet Nam. Mater Today Proc. https://doi.org/10.1016/j.matpr.2023.05.155
Wang L, Hou JL, Ou JP (2012) Moving force identification based on load shape function for a long-span bridge structure. Chin J Comput Mech 29:153–158
Wang W, Xiang Z, Wang Y, Shao X, Lu J (2024) Prestress force and general excitation identification for plate-like concrete bridges. Buildings 14:2032. https://doi.org/10.3390/buildings14072032
Wu SQ, Law SS (2010) Moving force identification based on stochastic finite element model. Eng Struct 32:1016–1027. https://doi.org/10.1016/j.engstruct.2009.12.028
Xiang Z, Chan THT, Thambiratnam DP, Nguyen T (2016) Synergic identification of prestress force and moving load on prestressed concrete beam based on virtual distortion method. Smart Struct Syst 17:917–933. https://doi.org/10.12989/sss.2016.17.6.917
Xiang Z, Chan THT, Thambiratnam DP, Nguyen T (2017) Prestress and excitation force identification in a prestressed concrete box-girder bridge. Computers Concrete 20:617–625. https://doi.org/10.12989/cac.2017.20.5.617
Yan M, Yang Y, Li X, Bao Y, Sun J, Sun B (2021) Pretensioned prestress friction losses considering contact imperfection at deviators in prestressed concrete girders. Struct Infrastruct Eng 17:1639–1650. https://doi.org/10.1080/15732479.2020.1821719

Yang IH (2005) Uncertainty and updating of long-term prediction of prestress forces in PSC box girder bridges. Comput Struct 83:2137–2149. https://doi.org/10.1016/j.compstruc.2005.02.030
Yang M, Gong J, Yang X (2020) Refined calculation of time-dependent prestress losses in prestressed concrete girders. Struct Infrastruct Eng 16:1430–1446. https://doi.org/10.1080/15732479.2020.1712438
Yau J-D, Yang Y-B, Kuo S-R (1999) Impact response of high-speed rail bridges and riding comfort of rail cars. Eng Struct 21:836–844. https://doi.org/10.1016/S0141-0296(98)00037-6
Zhang H, Guo Q-Q, Xu L-Y (2023) Prediction of long-term prestress loss for prestressed concrete cylinder structures using machine learning. Eng Struct 279:115577. https://doi.org/10.1016/j.engstruct.2022.115577
Zhou H, Fan X, Liu Y (2024) Dynamic serviceability and safety reliability analysis of aging PC girder bridges with non-prestressed reinforcement considering concrete shrinkage, creep and stochastic vehicle load flows. Structures 64:106515. https://doi.org/10.1016/j.istruc.2024.106515
Zhu J, Meng Q, Shi T, Yang X (2023) Long-term deformation analysis of prestressed concrete bridges under ambient thermal and vehicle loads. Struct Infrastruct Eng 19:1656–1675. https://doi.org/10.1080/15732479.2022.2052909

Publisher's Note

Springer Nature remains neutral with regard to jurisdictional claims in published maps and institutional affiliations.